Interactive role of rolling friction and cohesion on the angle of repose through a micro-scale assessment

Thao Doan

BEng (Hons)

PhD Candidate, Transport Research Centre, University of Technology Sydney, NSW 2007. Australia.

ORCID ID: https://orcid.org/0000-0003-0229-8376

Buddhima Indraratna[1]

PhD (Alberta), MSc (Lond.), BSc (Hons., Lond.), DIC, FTSE, FIEAust., FGS, CEng, CPEng

Distinguished Professor of Civil Engineering, Founding Director of Australian Research Council's Industrial Transformation Training Centre for Advanced Technologies in Rail Track Infrastructure (ITTC-Rail), Director of Transport Research Centre, School of Civil and Environmental Engineering, University of Technology Sydney, NSW 2007, Australia.

ORCID ID: https://orcid.org/0000-0002-9057-1514

[1]Corresponding author e-mail: buddhima.indraratna@uts.edu.au

Thanh Trung Nguyen

PhD, CPEng, M.ASCE, M.EAust

Research Fellow, Transport Research Centre, School of Civil and Environmental Engineering, University of Technology Sydney, NSW 2007, Australia.

ORCID ID: https://orcid.org/0000-0001-6078-2559

Cholachat Rujikiatkamjorn

PhD, MEng (AIT), BEng (Hons)

Professor, Transport Research Centre, School of Civil and Environmental Engineering, University of Technology Sydney, NSW 2007, Australia.

ORCID ID: https://orcid.org/0000-0001-8625-2839

Abstract

Cohesion and rolling friction play key roles in governing the behaviour of soil, however, only a limited number of studies have been able to assess the simultaneous contributions of these two micro-parameters on the macro-properties of soil. In this respect, the innovation of the current study includes an attempt to examine the interplay of these two primary parameters on the angle of repose (AoR) based on the discrete element method (DEM). Lifting cylinder tests on cohesive wet sand have been carried out in DEM, while the cohesion and rolling friction are captured through proposed computational models. In this paper, macro-parameters such as the geometry and developmental stages of sand piles obtained in DEM simulation are compared to experimental data, while their micro-evolution is quantified in detail. The results show that a large AoR can only be obtained when the cohesive and rotational frictional forces work in tandem. Increasing the cohesion and rolling friction results in smaller contact numbers with increasing chain-like connections between particles and larger pore spaces to account for a larger AoR. For the first time, this study distinctly identifies three major stages that contribute to the AoR, based on the development of contact numbers and the transformation of energy. Accordingly, the linkage between macro-scale AoR and the micro-structural coordination number is formulated with varying levels of cohesion and rolling friction. The DEM results prove that the more cohesive the particles are, the greater the delay in the dissipation of kinetic energy.

Keywords: cohesion, angle of repose, energy transformation, rolling friction, cohesive forces

1. Introduction

Soils are inherently particulate, which means their macroscopic behaviour is governed by collective microscopic interactions such as the frictional and cohesive contacts between discrete particles. In essence, cohesion arises in various forms that mainly include van der Waals forces between fine particles (Chen and Anandarajah 1996; Hamaker 1937), capillary forces in wet particles (Roy et al. 2016; Schwarze et al. 2013), and electrostatic forces (Matsusaka et al. 2010). Friction induced by sliding and rolling components is an essential aspect of particulate geomaterials due to the irregular shapes and surfaces of particles in nature. Obviously, the larger the angularity and roughness of particles, the larger the frictional resistance. A great deal of effort through advanced experimental and numerical approaches has been made to characterize the role that friction and cohesion has on the macro-behaviour of geomaterials. Of those studies, the use of discrete element method (DEM) has proved to be an effective and reliable approach of advancing our knowledge of various particle-scale behaviours of soil; for example, non-linear deformation under applied loads (Yimsiri and Soga 2010); stress state evolution (O'Sullivan 2011; Potyondy and Cundall 2004); granular breakage and settlement (Chen et al. 2022; Einav 2007; Huang and Tutumluer 2011; Nguyen et al. 2017); filtration and internal erosion (El Shamy and Zeghal 2005; Indraratna et al. 2021; Nguyen and Indraratna 2020; Tao and Tao 2017; Wu et al. 2021; Yin et al. 2021; Zhao and Shan 2013); and among others. Nevertheless, most previous DEM studies have been carried out on cohesionless granular soils even though cohesion has had a significant influence on the response of soil in a wide range of contexts. This means that more effort is needed in DEM to simulate cohesive soils more accurately and realistically.

Despite the clear physical mechanisms of particle cohesion, the effort to include cohesive forces in DEM models remains limited due to its complexity and excessive computation. Hence, it is common practice in DEM to utilize cohesion contact models such as

74 the JKR (Johnson-Kendall-Roberts) (Johnson et al. 1971) and the DMT (Derjaguin-Muller-
75 Toporov) (Derjaguin et al. 1975) models where different attractive forces are presented through
76 several simplified parameters. While JKR theory is considered to be more appropriate for soft
77 materials with large particles where the attractive forces are observed experimentally to only
78 appear inside the enlarged contact area, DMT theory is better suited to hard materials where
79 attraction only appears on the outside of the contact region (Barthel 2008; Prokopovich and
80 Perni 2011). Past studies (Johnson and Greenwood 1997; Li et al. 2011) have stated that the
81 JKR equation gives a decent prediction of contacting area with cohesive forces, compared to
82 the various experimental conditions.

83 In contrast to the above, the frictional behaviour of particles and its impact on the
84 macro-behaviour of soils have been investigated extensively; for example, the shear resistance
85 (Belheine et al. 2009; Muftah and Gutierrez 2010), granular flows (Goniva et al. 2012; Shan
86 and Zhao 2014), and rockfalls (Gentilini et al. 2012; Thoeni et al. 2014). Previous micro-
87 scanning studies (Nguyen and Indraratna 2020; Zhou et al. 2017) have shown that the
88 roundness and angularity indices of particles such as sand can vary from 0.5 to 0.8, a range that
89 can result in having a significant frictional resistance. The contribution made by rolling and
90 sliding friction on the overall response of geomaterials can change considerably depending on
91 the context, thus requiring specific justification when modelling. In highly confined systems
92 where soil shears under confinement, the sliding friction is significant, whereas rolling
93 resistance can dominate in uncompacted materials where particles have greater degrees of
94 freedom. For instance, when rock particles are falling down a slope, their rolling resistance
95 which depends mainly on the shape characteristics of the particles will govern how the particles
96 travel and transport kinetic energy in the system.

97 Although previous DEM studies have investigated the effect that rolling friction and
98 cohesion has on the behaviour of soil, their combined influence on the response of soil has

rarely been studied, especially in the case of fine or wet particles where cohesive forces become increasingly more dominant in relation to the self-weight of particles. Therefore, this study aims to close this gap by examining the importance of these parameters on the angle of repose (AoR), which is one of the most fundamental parameters used to characterize the frictional response of geomaterials in a naturally forming state, i.e., the steepest angle that soil can make in its loosest state, without slumping (Terzaghi 1943). This parameter is also used to present the morphology and internal friction of particulate materials, both of which have valuable implications for practical designs such as slope stability and retaining walls. Previous investigations (Grima 2011; Roessler and Katterfeld 2019) reveal that rolling friction and cohesion play significant roles in AoR of geomaterials, however, these studies normally use single values for these parameters and evaluate them individually, which gives an incomplete understanding of their interactive role in governing soil behaviour. It is noteworthy that while sliding friction can also affect the response of soil particles in forming the AoR, this influence is usually insignificant compared to rolling friction and cohesion (Carstensen and Chan 1976; El-Kassem et al. 2021; Meier et al. 2019; Zhou et al. 2001).

The current study employs DEM incorporated into the open-source software named LIGGGHTS (Kloss and Goniva 2011) to investigate the interactive roles of cohesion and rolling friction on the angle of repose. The macro-scale results are then validated against the experimental data, while the variation of micro-scale parameters is captured and analyzed. Based on these outcomes, this study attempts to link microscale elements to the conventional macro-parameter AoR, while tracking the energy transformation during the formation of AoR, which are key innovations.

2. Theoretical background

The governing equations of the discrete element method (DEM) used to model particle motion are given by:

$$m_i \frac{d\boldsymbol{v_i}}{dt} = \sum_{j=1}^{n_i^c} \left(\boldsymbol{F_{ij}^n} + \boldsymbol{F_{ij}^t} + \boldsymbol{F_{ij}^{coh}} \right) + \boldsymbol{F_i^g} \tag{1}$$

$$I_i \frac{d\boldsymbol{\omega_i}}{dt} = \sum_{j=1}^{n_i^c} \left(\boldsymbol{R_i} \times \boldsymbol{F_{ij}^t} + \boldsymbol{M_{ij}^r} \right) \tag{2}$$

where m_i and I_i are the mass and moment of inertial particle i respectively; $\boldsymbol{v_i}$ and $\boldsymbol{\omega_i}$ are the translational and angular velocities of particle i; $\boldsymbol{F_{ij}^n}$ and $\boldsymbol{F_{ij}^t}$ are the normal and tangential contact forces induced on particle i by particle j; $\boldsymbol{F_{ij}^{coh}}$ is the cohesive force between particle i and particle j while $\boldsymbol{F_i^g}$ is the gravitational force acting on particle i; $\boldsymbol{R_i}$ is the radius vector connecting the centre of particle i and the point of contact where the tangential force is initiated; $\boldsymbol{M_{ij}^r}$ is the rolling resistance torque induced to oppose the rotational interaction between particles i and j; and n_i^c is the number of contact of particle i.

Previous studies (Li et al. 2005; Zhu et al. 2007) have successfully used the nonlinear Hertz-Mindlin contact model to simulate granular materials, so this contact model is adopted in this current study. The normal and tangential contact forces (i.e., $\boldsymbol{F_{ij}^n}$ and $\boldsymbol{F_{ij}^t}$) derive from the corresponding contact stiffnesses (i.e., k_n and k_t) as follows:

$$k_n = \frac{4}{3} E^* \sqrt{R^* \boldsymbol{\delta_n}} \tag{3}$$

$$k_t = 8 G^* \sqrt{R^* \boldsymbol{\delta_n}} \tag{4}$$

where E^*, G^* and R^* are the equivalent Young's modulus, shear modulus, and the radius of two particles respectively, and $\boldsymbol{\delta_n}$ is the normal overlap or displacement vector. The determination of these parameters can be found in other studies (Li et al. 2005; Zhu et al. 2007).

In this study, to include the effect of rolling resistance, the elastic-plastic spring-dashpot (EPSD2) was used (Ai et al. 2011). Wensrich and Katterfeld (2012) stated that the EPSD2 model can be modified to accommodate a higher value of rolling stiffness; this can overcome the oscillatory behaviour and eliminate the need to consider rolling damping. The rolling resistance torque proposed by Iwashita and Oda (1998) can be computed with respect to the rolling friction coefficient μ_r as follows:

$$\left|\boldsymbol{M}_{\boldsymbol{ij}}^{\boldsymbol{r}}\right| \leq \mu_r R^* \left|\boldsymbol{F}_{\boldsymbol{ij}}^{\boldsymbol{n}}\right| \tag{5}$$

One of the most common cohesive models is the JKR model (Johnson et al. 1971), which has been modified from the classic Hertz (1881) contact model to consider the tensile forces at the contact edges. This model uses the concept of surface energy to represent the collective action of all the cohesive forces (i.e., the van der Waals, electrostatic, and capillary forces). The JKR model has been used extensively across different disciplines to model fine and wet sticky materials (Barthel 2008; Deng and Davé 2013; Louati et al. 2019). The governing equations of the JKR model are described as follows (Barthel 2008):

$$\boldsymbol{F}_{\boldsymbol{ij}}^{\boldsymbol{coh}} = \frac{4E^* a^3}{3R^*} - 2\sqrt{2\pi E^* \gamma a^3} \tag{6}$$

$$\boldsymbol{\delta}_{\boldsymbol{ij}}^{\boldsymbol{coh}} = \frac{a^2}{R^*} - \sqrt{\frac{2\pi a\gamma}{E^*}} \tag{7}$$

where $\boldsymbol{F}_{\boldsymbol{ij}}^{\boldsymbol{coh}}$ and $\boldsymbol{\delta}_{\boldsymbol{ij}}^{\boldsymbol{coh}}$ are the cohesive force and the deformation vector based on JKR theory between particles *i* and *j*; a is the enlarged contact radius, and γ is the equivalent surface energy. For simplicity, the JKR model can be modified into a linear cohesion model called SJKR, in which the surface energies, elastic modulus, and contact radius are combined into a single numerical parameter called Cohesion Energy Density (CED). In this simplified approach, the cohesive force is a product of CED (J/m^3) and the contact area A which is given by:

$$\boldsymbol{F}_{\boldsymbol{ij}}^{\boldsymbol{coh}} = CED.A \tag{8}$$

$$A = \pi a^2 = \frac{\pi}{4d^2}(4d^2R_1^2 - (d^2 - R_2^2 + R_1^2)^2) \quad (9)$$

where R_1 and R_2 are the radii of two contacting particles, and d is the distance between the centroids of the particles.

3. Numerical procedure

Due to its simplicity, the lifting cylinder test (or slump test) is the preferred method for determining the AoR of geomaterials (Lajeunesse et al. 2004; Rackl et al. 2017). A series of lifting cylinder tests were therefore carried out using DEM to investigate the combined effect of cohesion and rolling friction on the AoR. Sandy soils in dry and wet states commonly used in previous laboratory investigations were also used in this current study. By conducting lifting cylinder tests on various particle and cylinder sizes, Roessler and Katterfeld (2019) concludes that the use of up-scaled particles is a timesaving approach without a significant effect on the AoR value. On this basis, up-scaled particles were also used in this current investigation (Fig. 1). The SJKR model was used to simulate the cohesive behaviour of wet sand where the main underlying mechanism is governed by the presence of liquid bridges which leads to the development of capillary and viscous forces. While the SJKR model can be used to capture the capillary force, the effect of viscous forces can be compensated for by using the low restitution coefficient (i.e., 0.2), as demonstrated in previous studies (Behjani et al. 2017).

Initially, a sample of 7000 particles was generated randomly to fill a cylinder and then allowed to stabilize under gravity. The insertion phase was satisfied when the particles became fully static (i.e., the average velocity of particles was less than 0.5 mm/s). After stabilization, the cylinder was lifted at 0.008 m/s to maintain a quasi-static flow condition and prevent the particles from plashing downwards (Hassanzadeh et al. 2020). The simulation was completed when the kinetic energy of the pile reached a minimal value. A schematic of this lifting cylinder test is shown in Fig. 2. When the soil particles are completely contained inside the cylinder,

180 the boundary provides confinement through the particle-wall (P-W) contact that helps to
181 sustain particle frictional contact (P-P contacts) and prevent them from moving (see Fig. 2a).
182 It is noteworthy that the particle-wall contact was assumed the same for both sidewall and floor.
183 When the cylinder is lifted upwards, the particles lose their contacts due to the loss of boundary
184 confinement (see Fig. 2b), and then migrate laterally under gravitational force. It is apparent in
185 this process that the particles roll over each other and become displaced radially. As the
186 cohesion and/or rolling friction increases, the P-P contact forces are enhanced and the AoR
187 changes accordingly. The following sections present the numerical results with varying
188 cohesion and rolling friction, and an extensive analysis and discussion.

189 Since this study mainly focuses on rolling friction and cohesion where their input
190 parameters were varied, other DEM parameters were assumed based on selected previous
191 studies. For example, experimental validation by Roessler and Katterfeld (2019) showed that
192 the particle-wall friction coefficient could vary from 0.35 for the contact between sand and
193 steel to 0.37 for the contact between sand and plastic. Accordingly, the current study adopted
194 an average value of 0.36. Moreover, the shear modulus value was reduced to $10x10^7$ (Pa) to
195 enhance computational efficiency, whilst noting that this assumption would not affect the
196 contact behaviour of sand particles with respect to the unconfined state of soil during an AoR
197 test (Lommen et al. 2014). The DEM input parameters are summarised in Table 1.

198 To approximate the range of rolling friction, this study followed the empirical
199 formulation provided in Ucgul et al. (2014), which resulted in the coefficients of rolling friction
200 varying from 0.05 to 0.4 for sand, with a radius varying from 0.1 to 10 mm. Since in previous
201 studies (Derakhshani et al. 2015; Liu et al. 2018; Phan et al. 2021) where the coefficient of
202 rolling friction for granular materials varied from 0.1 (relatively rounded particles) to 0.5
203 (crushed angular particles), the same range was adopted for the current numerical simulations.
204 The selection of CED values was based on previous DEM studies which simulated wet and

205 sticky granular materials. For example, Grima (2011) correlated the value of CED based on an
206 approximation of tensile stress (Rumpf 1962), and then proposed a CED from 0 to 3.5 x 10^6
207 (J/m^3) for wet washed coal. Roessler and Katterfeld (2019) estimated a CED from 4.6 x 10^6 to
208 5.4 x 10^6 (J/m^3) for wet sands, with a moisture content of 9.5% and a bulk density of 2083
209 kg/m^3. The current study used a CED ranging from 0 for non-cohesive materials to 5 x 10^6
210 (J/m^3) for highly cohesive assemblies. The range of rolling friction coefficients and CED are
211 shown in Table 2.

212 # 4. Results and Discussion

213 ## 4.1 Comparison of DEM results with experimental observation

214 Figure 3 shows four phases of the simulated lifting cylinder test for a given lifting height (h),
215 which is the gap between the lower boundary of the cylinder and the horizontal base (i.e., h =
216 90 mm, 120 mm, 160 mm and 280 mm for a 375mm high cylinder). The result shows that the
217 flow characteristics of the simulated wet sand are comparable with the experimental outcomes
218 by Roessler and Katterfeld (2019), as highlighted in the enclosed areas marked with a red dash.
219 Generally, there are four different stages in forming the angle of repose (AoR) considering
220 experimental observations. The first stage (h = 90mm), shows a stable column of material in
221 the DEM simulation without any bend or materials breaking out. This observation agrees with
222 the experimental findings by Roessler and Katterfeld (2019) where repeated tests showed that
223 wet sand had a consistent shape for the given lifting height. As the gap increases to 120 mm, a
224 slight bending of wet sand could be seen numerically and experimentally (Stage 2). With a
225 160mm height gap, the simulations and experiments indicate that the materials spread outwards
226 to form a convex slope (Stage 3), and when the gap reaches 280mm (Stage 4), there is a stable
227 formation of cohesive sand as indicated experimentally and numerically. The four stages in the
228 development of AoR of wet sand (Fig. 3) corroborated well through both experimental and

DEM simulations. The only difference between the numerical and experimental results was that the numerical method could not simulate the cracks occurring while the wet sand expanded laterally due to the non-uniformity distribution of water content and liquid-bridging forces between soil particles in the experiment.

To obtain a quantitative comparison, for a lifting height between 80 mm to 140 mm (i.e., h = 80, 100, 120 and 140 mm), the pile diameters (d_{pile}, defined by a yellow horizontal dash line in Fig. 4a) corresponding to each 20 mm predefined slice height were extracted to evaluate the spread of materials outside the column. The relative pile diameters (d_{rel}) were computed relative to the diameter of the cylinder ($d_{cylinder}$) to demonstrate the percentage of convex bending of the sand pile. The formulation of d_{rel} is determined as follows:

$$d_{rel} = \frac{d_{pile-}d_{cylinder}}{d_{cylinder}} x100\ (\%) \tag{10}$$

Figure 4b shows that the relative diameters of the piles for a given lifting height, as obtained by the current simulations and experiments, agree very well. For instance, with a lifting height where h=80mm, the simulated pile remains almost vertical with 2.3% convex bending, compared to 2.1% bending in the laboratory measurements. As the lifting height increases to 140mm, the percentage of bending in the simulation increases to 25.1%, compared to 25% in the test case. Exceeding the gap height further led to inconsistent bending of the material (Roessler and Katterfeld 2019), and therefore it was not considered. In essence, the DEM simulations successfully captured the main features of the experimental outcomes (see Fig. 3) and depicted the quantitative relationship between the lifting height and the percentage of convex bending (Fig. 4b).

4.2 The effect of rolling friction coefficient and cohesion on the angle of repose

Based on the final configuration of the simulated piles, the final height and the average radius of the pile were computed to determine the approximate values of the angle of repose (AoR)

252 with respect to the method given by Kermani et al. (2015). As summarised in Table 3 and Table
253 4, rolling friction coefficients and cohesion have a considerable effect on the value of AoR,
254 such that as the rolling friction and cohesion increase, the final pile is higher and slimmer,
255 implying that the angle of the slope is higher. Table 5 shows that without cohesion (i.e., CED
256 = 0), AoR varies between 27 to 35 degrees for a system of spherical particles where the
257 coefficient of rolling friction varies from 0.1 to 0.5, respectively. This range of AoR agrees
258 with the average angle of the slope of dry sand piles reported in previous experimental studies;
259 for example, 34^0 in (Beakawi Al-Hashemi and Baghabra Al-Amoudi 2018; Derakhshani et al.
260 2015) and 29.7^0 for Toyoura sand (Nakashima et al. 2011). This result attests to the dependency
261 of the macroscopic AoR on the microscopic rolling resistance of individual particles
262 (Derakhshani et al. 2015; He et al. 2021; Hoshishima et al. 2021). A higher rolling resistance
263 means particles consume more kinetic energy, which leads to the formation of heaps with a
264 high potential (Zhou et al. 2001). Moreover, the opposition to the rotational movement of
265 particles helps prevent them being rearranged due to gravity, which leads to a higher build-up
266 of particles.

267 Table 5 also shows that an increasing level of cohesion gives rise in the AoR for all
268 levels of rolling friction. Several past studies (Mason et al. 1999; Mitarai and Nori 2006)
269 indicate that for a given material, the slope angle of a wet assembly is always higher than a dry
270 system, however, they did not investigate how varying the degree of cohesion can affect the
271 response of this slope angle. The simulated AoR can reach from 40 to 45^0, which agrees with
272 the values of wet cohesive sand piles reported previously (Beakawi Al-Hashemi and Baghabra
273 Al-Amoudi 2018). Nase et al. (2001) observed the effect of cohesion on the flowability of
274 materials and indicated that the more cohesive it is, the less “flowable” is the system because
275 the additional cohesive force induced by liquid prevents particles from sliding and rolling on
276 an inclined surface and helps to form a stable structure.

277 The contour graph in Fig. 5 shows the coupled influence of rolling friction and cohesion
278 on the AoR outcomes. Notably, each contour line has a similar tendency where a steep slope
279 initially occurs followed by a flattening behaviour when the rolling friction or cohesion
280 becomes dominant. This postulates that when the rolling friction is insignificant, the AoR
281 results do not vary as much with the levels of cohesion, and vice versa. Therefore, a large AoR
282 can only be accomplished when the rolling friction and cohesion work in tandem.

283 ## 4.3 Variations of porous feature with degrees of cohesion and rolling friction

284 The overall porosity is an important macroscopic parameter which is governed by microscopic
285 parameters such as particle size and inter-particle forces. Given its significance, this study
286 applied a numerical algorithm based on the Monte-Carlo approximation to estimate the
287 porosity within a volumetric region. The theoretical background of a Monte-Carlo
288 approximation can be found elsewhere (Amberger et al. 2012; Campillo et al. 2021). To
289 implement Monte-Carlo algorithms, a Python program is developed to apply a 'hit-and-run'
290 approach and arbitrary walks into the representative volume element (RVE) of the final pile of
291 sand. The RVE samples were chosen to be sufficiently large enough to contain at least 1000
292 particles, and they proved to yield macroscopically reasonable results (Wiącek et al. 2012).
293 With this technique, the porosity of a certain region can be computed without knowing its
294 specific geometric features and the boundary conditions which are usually required in
295 conventional analytical methods.

296 Figure 6 shows the variation of porosity which was initially 0.54 and changed with
297 different levels of rolling friction coefficient and cohesion. It illustrates that a more porous
298 structure is obtained when the rolling resistance and cohesive forces become larger. With a
299 higher coefficient of rolling friction, the porosity increases proportionally irrespective of the
300 level of cohesion. Specifically, without cohesion (i.e., the black solid line), porosity changes

from 0.586 to 0.602 when the rolling friction coefficient increases from 0.1 to 0.5. The same influence also repeats across different levels of cohesion. For example, in the case of very small rolling resistance (i.e., μ_r= 0.1), increasing CED from 0 to 5x10^6 (J/m^3) causes an increase in porosity from 0.586 to 0.600. This is understandable because when cohesion increases, the particulate structure of the material becomes progressively separated with larger voids (Deng and Davé 2013; Parteli et al. 2014; Thakur et al. 2014; Yang et al. 2000; Yu et al. 2003).

To elucidate the insightful mechanism of particle rearrangement of sand pile under increasing cohesion, cross-sections of the cohesionless and cohesive sand piles are shown in Fig. 7. When observing the contact numbers marked with different colours (i.e., from blue to red for smaller to larger contact numbers respectively), the number of touching particles increases from the edge of the pile to the centre. This phenomenon occurs because the central portion of the pile is mostly formed by vertically deposited particles, which undoubtedly have less freedom to displace, and hence contact more frequently with their neighbours. The result also indicates that when cohesion is present, the soil particles tend to bond to each other by attraction which promotes increasing chain-like connections and a more heterogeneous porous structure. For example, Fig. 7 shows that the particles and pores of the cohesionless sand pile are distributed more homogeneously, whereas larger pores are formed more frequently by chain-like connections (highlighted in red rectangles). This finding is corroborated with several past studies (Rognon et al. 2007; Xu et al. 2007) where cohesion creates a more non-uniform porous structure of particulate media. However, none of them showed quantitative changes in porosity due to the combined effect of cohesion and rolling friction given in this current study. The large voids observed in numerical cohesive systems can be correlated to a phenomenon known as increasing open micro-fabrics with cohesion, as reported in past experiments with mixtures of sand and clay (Goudarzy et al. 2021; Gratchev et al. 2006).

4.4 Micro-evolution of forming the angle of repose

In order to quantify changes in the micro-features of soil while forming the angle of repose (AoR), the total contact number (n_c), which was computed and outputted through DEM contact algorithm, represents how many contacts that a particle or group of particles have with each other. The larger the contact number, the more robust the particulate structure. Figure 8 shows how the total number of contacts in a sand pile change over time with different degrees of cohesion and rolling friction, based on current DEM investigations. These results show that despite different magnitudes of cohesion and rolling friction, there are three major stages in forming AoR. First, n_c decreases with time and there is no significant impact between cohesion and rolling friction during this initial stage, but then it experiences a state where the value fluctuates with time (i.e., a chaotic state) and the effects of cohesion and rolling friction become apparent. Finally, n_c becomes stable when the particles form stable slopes in accordance with different input values of cohesion and rolling friction. It is interesting that with a higher rolling friction, soil particles take longer to reach a chaotic stage; for example, when μ_r = 0.1, it takes about 6.5s whereas when μ_r = 0.4, it takes 10s. Moreover, the variation in rolling resistance leads to a change in the number of contacts. Figure 8 also shows that when μ_r increases from 0.1 to 0.4, the number of contacts decrease from 2.94×10^4 to 2.75×10^4 in the initial stage. In the context of small rolling resistance (i.e., μ_r = 0.1), the number of contacts decreases significantly from 2.8×10^4 to 2.6×10^4 when the CED increases from zero (i.e. cohesionless) to 5×10^6 (i.e. cohesion-dominated systems) (Fig. 8a). This declining number of contacts with cohesion also occurs when the rolling friction increases (i.e., μ_r = 0.4), as shown in Fig. 8b. This micro-scale development shows three major stages in forming AoR, unlike the four stages in the macro-scale (experimental) observations shown in Fig. 3. In fact, stages 1 and 2, where soil particles have not moved very much, as shown earlier in Fig. 3, can be combined into the initial stage based on the evolution of contact number.

350 The coordination number CN (i.e., an average number of contacts per particle) is
351 generally computed based on the total contact number (n_c) and particle number (n_p), as follows
352 (Thornton 2000):

$$CN = \frac{2n_c}{n_p} \tag{11}$$

353 Figure 9 shows a two-dimensional contour map to represent the interactive roles that rolling
354 friction and cohesion can have on the coordination number CN. In the absence of cohesion,
355 increasing the rolling friction from 0.1 to 0.5 leads to a reduction in the mean CN from 8 to
356 7.3. This range of CN values corresponds to the results obtained from previous studies on
357 cohesionless materials (Yang et al. 2000; Yu et al. 2003). The coupled effect of rolling friction
358 and cohesion also causes the CN to experience a continuous decline to reach values between 6
359 and 7 when both factors increase.

360 To further explain the interaction between cohesive and rolling resistant forces, as they
361 affect the coordination number, the equilibrium of all external and internal forces that act on
362 particles is explored. Yu et al. (2003) indicated that it is common for cohesionless granules to
363 have an average of six contacts per particle to stabilize the gravitational influence. However,
364 with increased rolling friction and cohesion, the combined magnitude of cohesive and frictional
365 forces is sufficient to resist the effect of gravitational forces. Therefore, stability can be
366 achieved with fewer interparticle contacts, which can be as minimal as two contacts per particle
367 (Xu et al. 2007). Figure 10a & Figure 10b show the distribution of contact numbers under
368 variations of cohesion and rolling friction, respectively. For μ_r = 0.2, highly cohesive material
369 (i.e., CED = 5x10^6) has the largest frequency of distribution, i.e., around 3 contacts per particle,
370 whereas non-cohesive material (i.e., CED = 0) experiences a more distributed peak of around
371 4 contacts per particle (Fig. 10a). On the other hand, without cohesion, Fig. 10b shows that
372 with lower rolling friction (i.e., μ_r = 0.1 shown as a solid black line), the frequency curve tends
373 to change to the right to account for the higher frequency of larger contact numbers (i.e., > 4

374 contact/particle). In general, the peak of the distribution curve shifts to the left with a lower
375 contact number when the cohesion and rolling friction of the system increase.

376 4.5 Energy transformation and particle displacement process

377 The process of energy transformation is theoretically recognized as an inherent characteristic
378 of dynamic particulate systems. Since the microscopic details of particles can be tracked over
379 space and time, DEM is now used to compute the energetic components of granular soils such
380 as the potential and kinetic energies (PE and KE) (Kermani et al. 2015; Nguyen et al. 2020;
381 Nguyen and Indraratna 2020). The potential and kinetic components are computed as follows:

$$E_p^t = \sum_{i=1}^{n_p} m_i g z_i^t \tag{12}$$

$$E_k^t = E_k^{translational} + E_k^{rotational} = \sum_{i=1}^{n} \frac{1}{2} m_i (v_i^t)^2 + \frac{1}{2} I_i (\omega_i^t)^2 \tag{13}$$

382 where z_i^t is the height of particle *i* with respect to the horizontal datum at time *t*.

383 When the simulated particles have settled inside a cylindrical column with a stabilized
384 kinetic energy, the total amount of energy is considered to be equal to the potential energy at
385 rest (t=0). The cylinder is then lifted, making the column of particles start to collapse and
386 resulting in an instantaneous exchange between the potential and kinetic energy of particles.
387 Figure 11a & Figure 11b reveal an apparent shift in the magnitude of potential energy over
388 time using different levels of cohesion (i.e., CED ranges from 0 to $5x10^6$) for two representative
389 cases of rolling friction 0.1 and 0.4. When the rolling friction is small (i.e., 0.1), the variations
390 of potential energy remain almost constant for the first 6-8 seconds, they then decrease
391 significantly for 8-16 seconds and finally reach a constant value after 16 seconds (see Fig. 11a).
392 This consistent trend of potential energy makes it a reliable criterion for signifying the stability
393 of granular heaps, as also recognized elsewhere (Zhou et al. 1999). Moreover, the magnitude

394 of potential energy for different levels of cohesion and rolling friction can be used to quantify
395 the slope feature of granular piles. For instance, the potential energy of a highly cohesive pile
396 (i.e., CED = $5x10^6$) has a higher value than for non-cohesive (CED = 0) and moderately
397 cohesive cases (see Fig. 11a & Fig. 11b). The higher potential energy at the final stage means
398 the slope has a steeper angle.

399 Figure 12a & Figure 12b show the variations of total kinetic energy (KE) in
400 cohesionless and cohesive systems at two levels of rolling friction (i.e., μ_r = 0.2 and 0.3). This
401 shows that the peak values of kinetic energy in the cohesionless system are higher than in cases
402 with cohesion. The larger the cohesion, the smaller the peak value of KE; this is because
403 increasing cohesive forces provides additional resistance against the movement of particles,
404 and hence reduces the kinetic energy. However, this variation cannot be generalized in every
405 case of cohesion and rolling friction due to difficulties in maintaining a quasi-static condition
406 and preventing the sticky particles from avalanching. Furthermore, the kinetic energy fluctuates
407 greatly with localised peaks when the wet sand column began to collapse. These fluctuations
408 are the result of a massive difference in magnitude between the computation of potential and
409 kinetic energies, and thus, with a slight change in particle elevation, the kinetic energy can be
410 varied significantly. It takes much longer to reach the peak and stabilize KE when cohesion is
411 added to the system, and this indicates that more time is needed for KE to dissipate in cohesive
412 material. For example, Fig. 12a shows that the cohesionless system takes about 17.5s to fully
413 stabilize, whereas cohesive systems take around 19 to 20s to reach the same state.

414 The total displacement of all particles in the sand piles is computed across different
415 levels of cohesion and rolling friction to further enhance our understanding of the evolution of
416 kinetic energy in the system. Figure 13 shows the results where μ_r = 0.2 and μ_r = 0.3, with
417 CED = 0 and $5x10^6$, both of which corroborate the behaviour of kinetic energy shown earlier.
418 Those particles without cohesion (black line) begin to migrate and reach the first peak earlier

than in the cohesive cases. For example, Fig. 13a shows that cohesionless particles begin to displace at around 6s, whereas soil particles with cohesion (CED = $5x10^6$) begin to migrate at approximately 7.5s. However, cohesionless particles stop travelling (stabilizing) at 18s, rather than the 21s when cohesion is included. Total displacement is highly susceptible to fluctuating peaks due to the sudden avalanching of cohesive and highly frictional particles. Figure 13b also shows that the largest peak of displacement that cohesionless particles can make is much higher than for the cases with cohesion; for example, 49.5m for non-cohesive material compared to 35 m for cohesive particles (i.e., CED = $5x10^6$). This indicates that the material becomes less brittle, i.e., the material reaches to lower peak deformation and takes longer time to stabilize the kinetic energy when cohesion is added.

4.6 Correlation between macro- and micro-parameters

This analysis has shown that the bulk-scale angle of repose (AoR) and particle-scale coordination number (CN) of the sand piles are a function of the levels of cohesion and rolling friction. Therefore, by appraising the overall dataset, the relationship between these two parameters (i.e., AoR and CN) in the two typical cases (i.e., the lower (μ_r = 0.1) and upper (μ_r = 0.5) rolling resistance with varying cohesion) can be formulated, as shown in Fig. 14a & Fig. 14b. These figures show that the fitted regression lines describe the relationship between AoR and CN very well, with a percentage of error less than 5%. These equations also illustrate the negative dependency of AoR on CN, thus indicating that the higher the average number of contacts per particle, the smaller the AoR values. It is generally understood that the average connection between each particle and its neighbours rises with densification, and vice versa (O'Sullivan 2011). This means that when CN increases, the gravity-induced densification and rearrangement of particles are enhanced considerably. In fact, as the effect of gravity increases, particles are more prone to moving, which leads to a smaller AoR. By contrast, as cohesion

443 increases, the governing effect of gravity and the process of densification are compromised,
444 leading to higher AoR and smaller CN values (i.e., when the CED increases, the AoR-CN
445 relationship follows an upward trend to the left, as shown in Fig. 14a & Fig. 14b). This
446 generalization is also applicable for all the other levels of rolling friction where μ_r ranges from
447 0.1 to 0.5.

448 ## 5. Conclusion

449 This study adopted the discrete element method (DEM) to investigate how cohesion and rolling
450 resistance could simultaneously affect soil behaviour considering the angle of repose (AoR).
451 Macro-parameters such as the geometry of the sand piles predicted by DEM compared quite
452 well with the experimental data, while the microscopic parameters were computed to further
453 understand the micro- and energy transformation of the systems. The innovation of this study
454 was that the systemic variations of cohesion and rolling friction in DEM allowed their coupled
455 effects on the macroscopic and microscopic levels to be captured, which were then used to
456 provide a linkage between the conventional AoR and the micro-scale elements. The salient
457 findings of this study are summarised as follows:

458 • The simulation results proved that the AoR was a function of cohesion and rolling
459 resistance, as represented by the contour plot. Increasing cohesion and rolling friction
460 resulted in a larger AoR, which can, for instance, reach 44° when CED = $5\text{x}10^6$ and μ_r =
461 0.5. When either of these parameters was insignificant, the dependency of AoR on another
462 was greatly reduced. Therefore, an angle with a steep slope can only be accomplished when
463 both cohesive and rotational frictional forces are high.
464 • The overall porosity of sand piles increased regardless of the level of cohesion when the
465 rolling friction increased, and vice versa. The cross-section of cohesive piles showed that
466 the soil became more heterogeneous with increasing chain-like bonds between particles

when cohesion increased, leading to larger porosity and a higher AoR. The coordination number at the peak frequency tended to decrease as cohesion between the particles of soil increased.

- The micro-analysis showed that the total and average contacts in the system (i.e., n_c and CN) significantly decreased when cohesion and rolling resistance dominated. When resistance was enhanced from cohesive and frictional actions, the particles needed less inter-particle contacts to counteract the gravitational forces, and thus resulting in a larger AoR. Based on the numerical data, empirical relationships ($R^2 > 0.98$) between the macro-parameter AoR and the micro-parameter coordination number (CN) were established for the first time by considering different degrees of cohesion and rolling friction.
- The variations in particle contact (via n_c) indicated that there were three major stages in forming the angle of repose, AoR. They were, (*i*) the initial stage where n_c dropped over time without any significant effects of cohesion and rolling friction, (*ii*) the chaotic stage during which n_c fluctuated significantly and the influences of cohesion and rolling friction became apparent, and (*iii*) the final stabilizing stage where n_c and the corresponding AoR set totally different levels in accordance with different degrees of cohesion and rolling friction.
- The analysis of energy transformation showed that the residual potential energy was larger as cohesion and/or rolling friction increased, which corroborated with the higher value of AoR. The kinetic energy and the corresponding displacements of particles became less significant as cohesion and/or rolling friction increased. The more cohesive the particles, the greater the delay in kinetic energy being triggered and dissipated (i.e., the less brittle the particle response), and the corresponding displacement.

Data Availability Statement

Some or all data, models or code that support the findings of this study are available from the corresponding author upon reasonable request.

Acknowledgements

This research was supported by Transport Research Centre (TRC, UTS), and the Australian Government through the Australian Research Council's Linkage Projects funding scheme (project **LP160101254**). Technical and financial support from industry partners including SMEC, Sydney Trains, ACRI and Coffey are greatly appreciated.

Tables

Table 1: DEM input parameters of simulated study

Parameters	Inputs	References
Particle density (kg/m^3)	2650	
Poisson's ratio	0.3	
Shear modulus (Pa)	10x10^7	
Restitution coefficient	0.2	(Behjani et al. 2017)
Particle-wall friction coefficient	0.36	(Roessler and Katterfeld 2019)
Particle-particle sliding friction	0.5	(Nguyen and Indraratna 2020; Phan et al. 2021)
Timestep (s)	10^{-5}	10% Rayleigh time step
Gravitational acceleration (m/s^2)	9.81	

503 Table 2: DEM calibration parameters

Parameters	**Value range**	**Value increment**
Rolling friction coefficient (μ_r)	0.1 - 0.5	0.1
Cohesion Energy Density (CED) (J/m^3)	0 - 5x10^6	1x10^6

504

505

506 Table 3: The final height of the material formation with varying cohesion and rolling friction

Height of the final pile (m)					
CED (J/m3) \ **Rolling friction**	0.1	0.2	0.3	0.4	0.5
0	0.1541	0.1644	0.1771	0.1910	0.1934
$1x10^6$	0.1542	0.1688	0.1788	0.2015	0.2078
$2x10^6$	0.1553	0.1763	0.1850	0.2102	0.2126
$3x10^6$	0.1594	0.1801	0.1911	0.2148	0.2196
$4x10^6$	0.1702	0.1849	0.2030	0.2196	0.2251
$5x10^6$	0.1703	0.1917	0.2107	0.2237	0.2273

507

508 Table 4: The average radius of the material formation with varying cohesion and rolling friction

Radius of the final pile (m)					
CED(J/m3) \ **Rolling friction**	0.1	0.2	0.3	0.4	0.5
0	0.3019	0.2858	0.2843	0.2725	0.2704
$1x10^6$	0.2883	0.2775	0.2826	0.2705	0.2651
$2x10^6$	0.2880	0.2726	0.2800	0.2655	0.2620
$3x10^6$	0.2883	0.2682	0.2730	0.2601	0.2584
$4x10^6$	0.2829	0.2670	0.2672	0.2401	0.2421
$5x10^6$	0.2674	0.2616	0.2567	0.2471	0.2217

509

510 Table 5: The variations of AoR with various levels of cohesion and rolling friction

Angle of repose (AoR) (degrees)					
CED(J/m3) \ Rolling friction	0.1	0.2	0.3	0.4	0.5
0	27.04	29.91	31.92	35.03	35.57
$1x10^6$	28.06	31.31	32.32	36.68	38.09
$2x10^6$	28.34	32.89	33.45	38.37	39.06
$3x10^6$	28.94	33.88	34.99	39.20	40.36
$4x10^6$	31.03	34.70	37.23	41.82	42.92
$5x10^6$	32.49	36.23	39.38	42.15	45.71

511

512 **Figures**

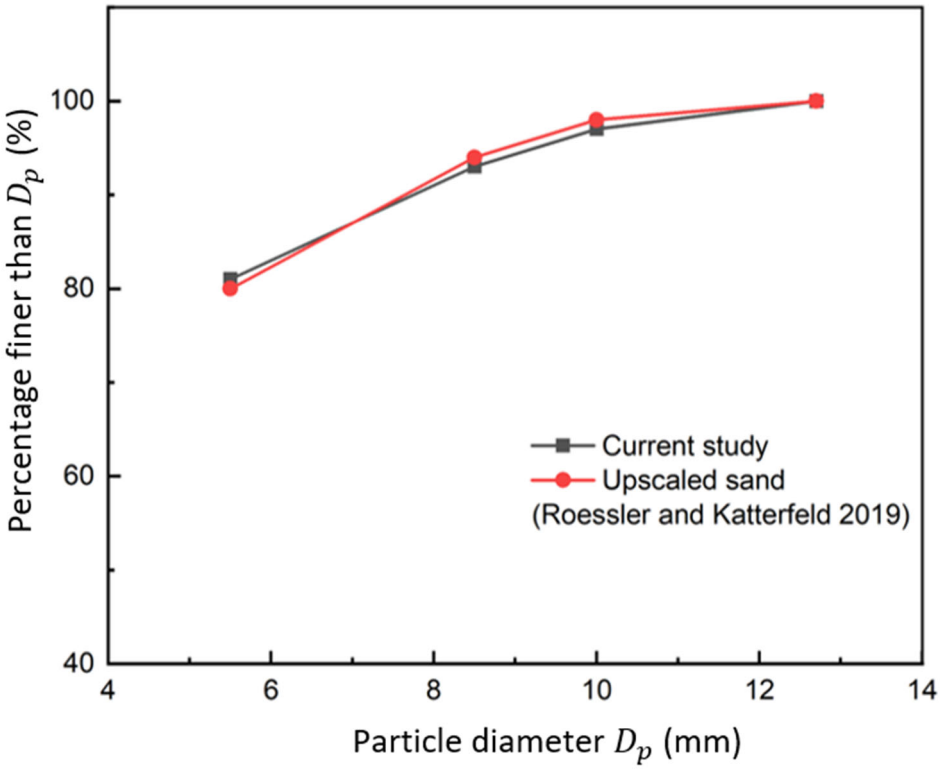

513

514 Fig. 1. Particle size distribution of simulated soil

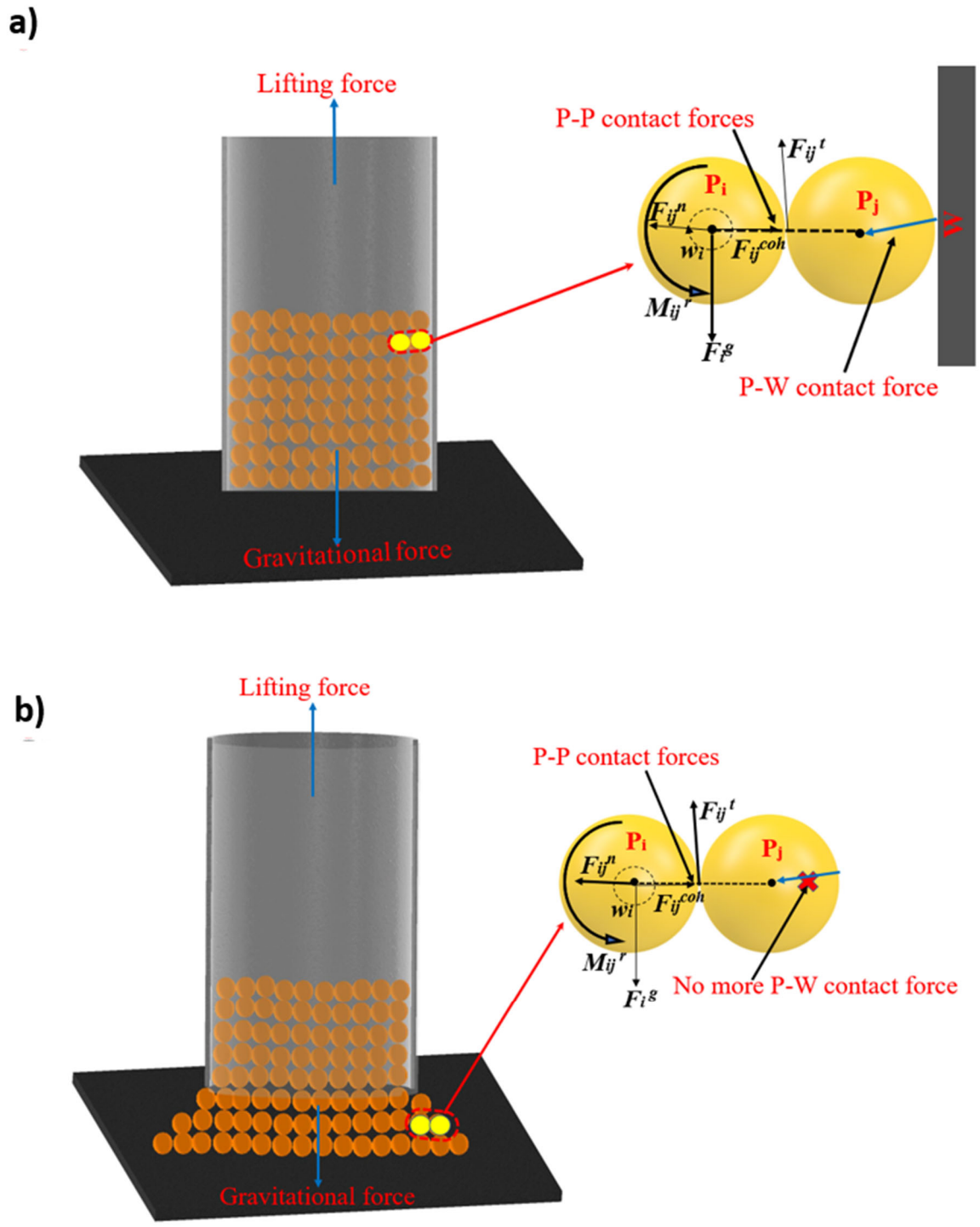

Fig. 2. The lifting cylinder test a) before lifting, b) during lifting

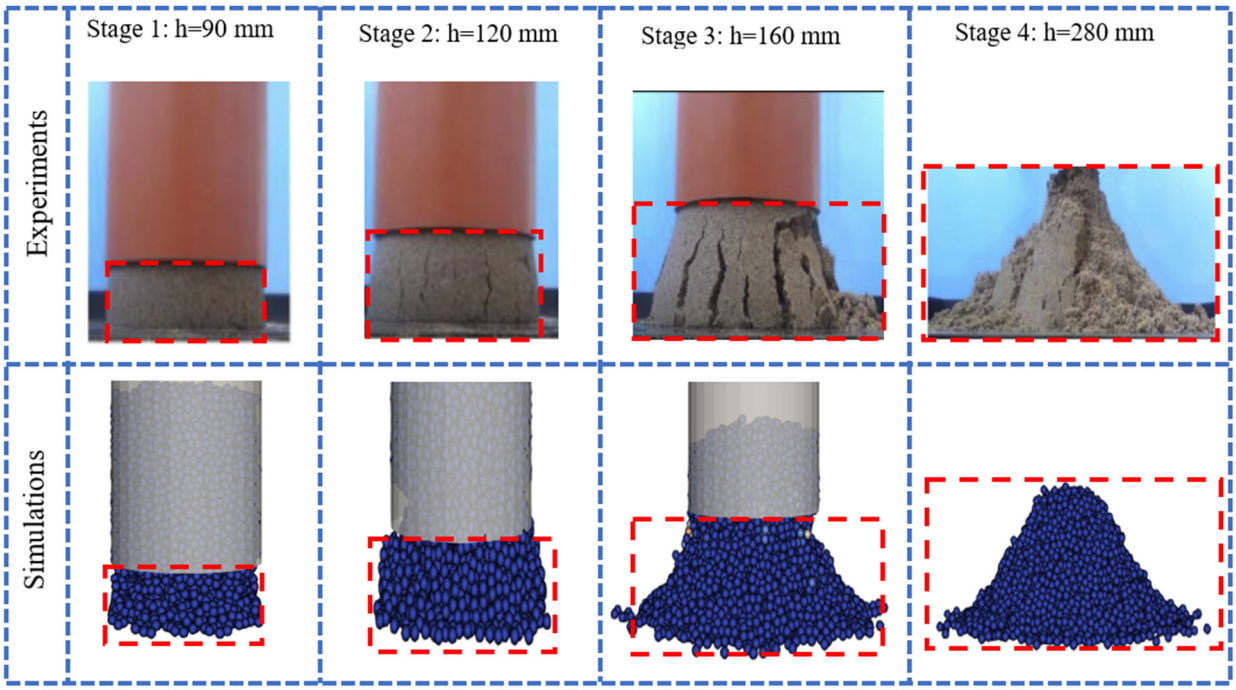

Fig. 3. Validation of the current simulated DEM (i.e., μ_r= 0.5, μ_s= 0.5 and CED = 5x10^6 J/m^3) with previous experiment results (Roessler and Katterfeld 2019)

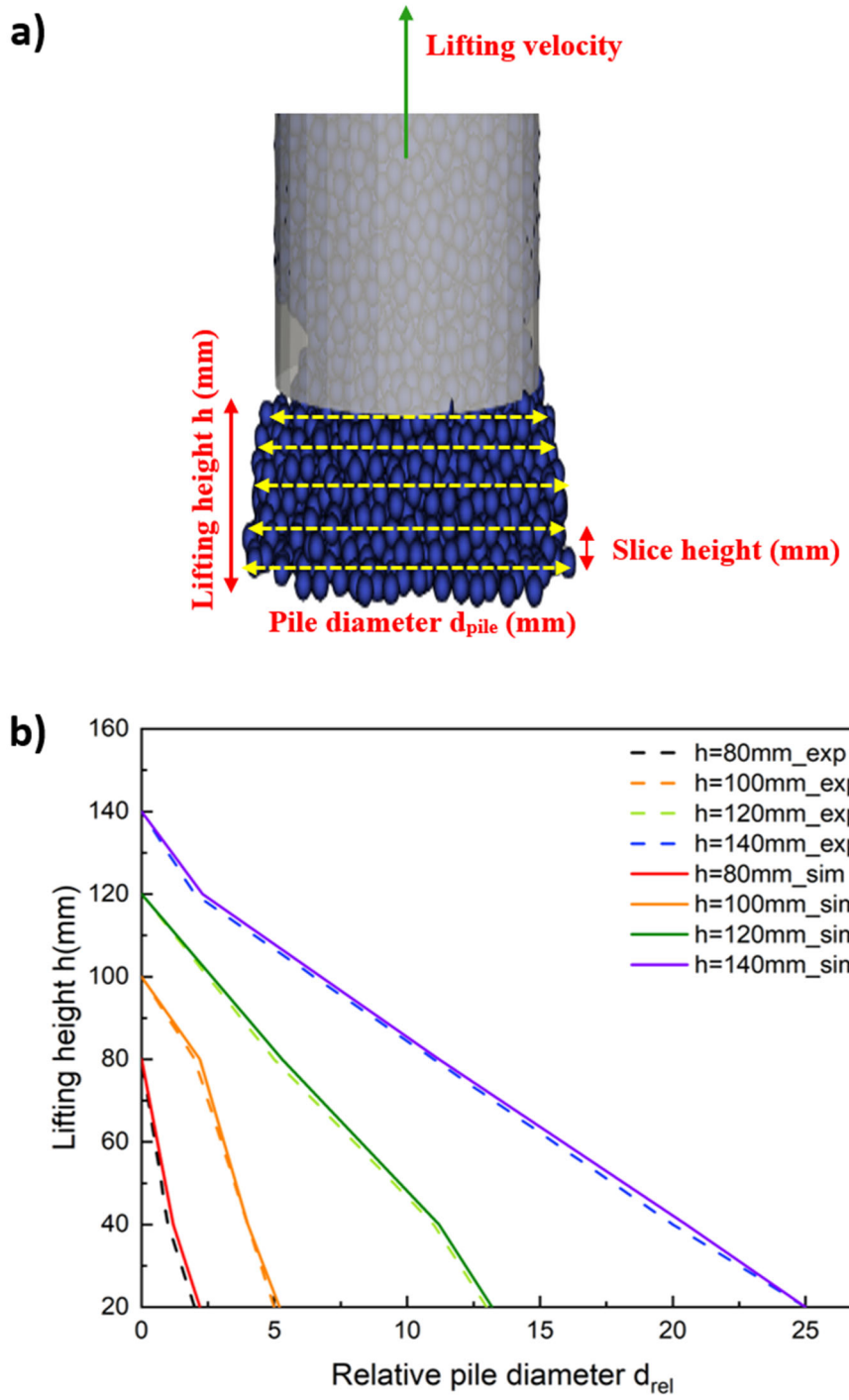

Fig. 4. a) Definition of lifting height and pile diameter, b) Lifting height versus relative diameter predicted by the current DEM in comparison with previous results by (Roessler and Katterfeld 2019)

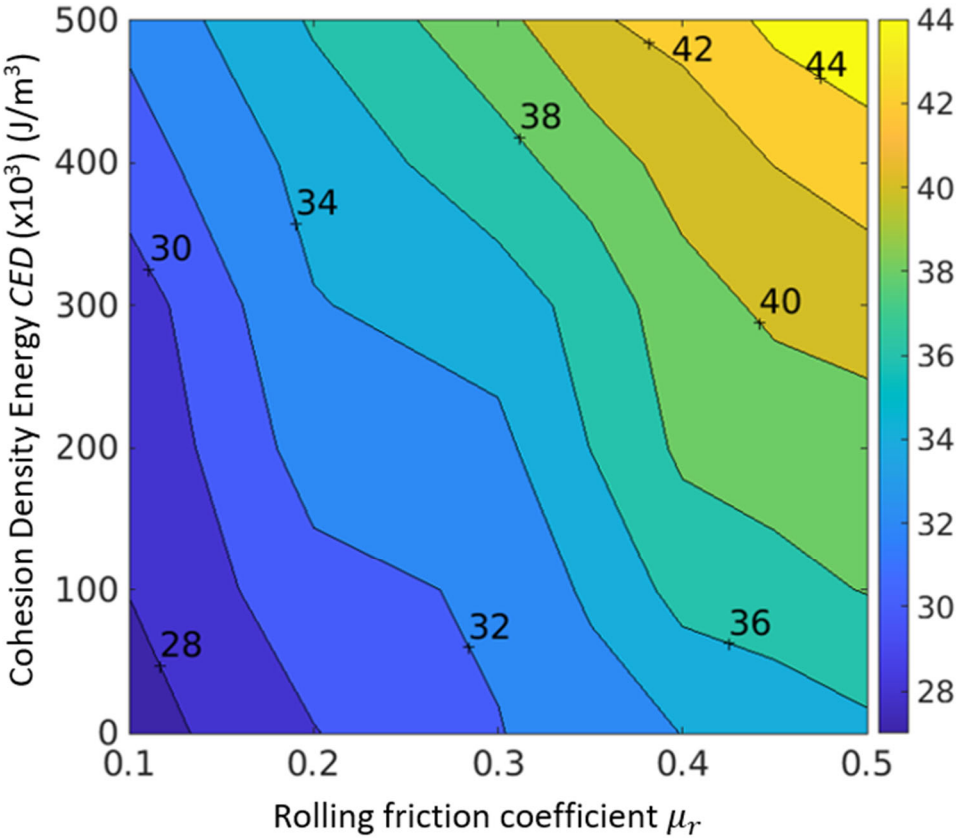

Fig. 5. Angle of repose as a function of cohesion (CED) and rolling friction

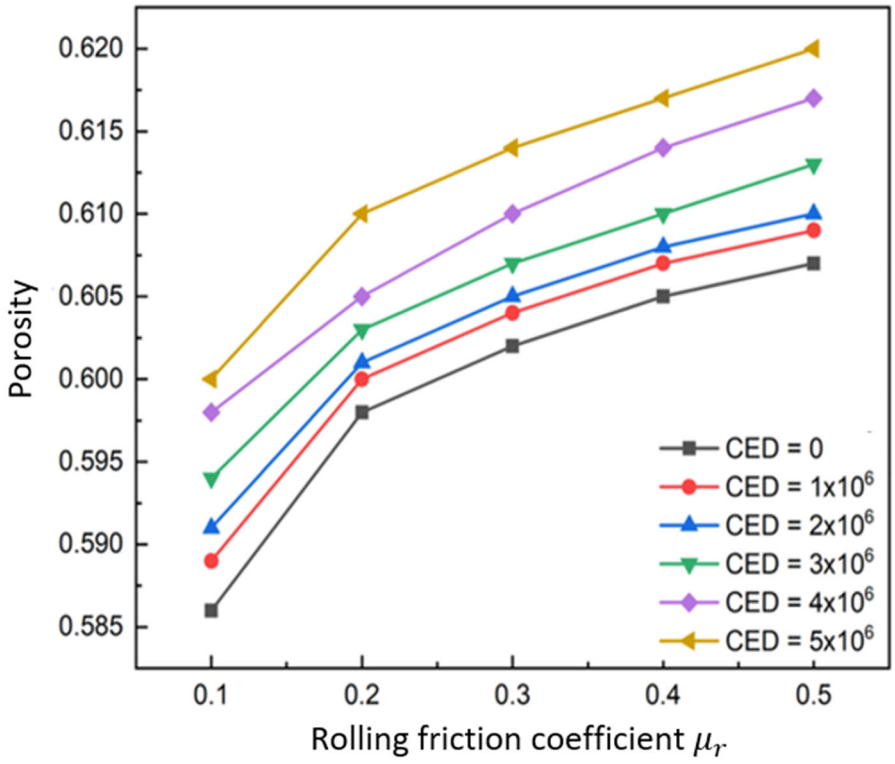

Fig. 6. Variations in porosity with cohesion and rolling friction

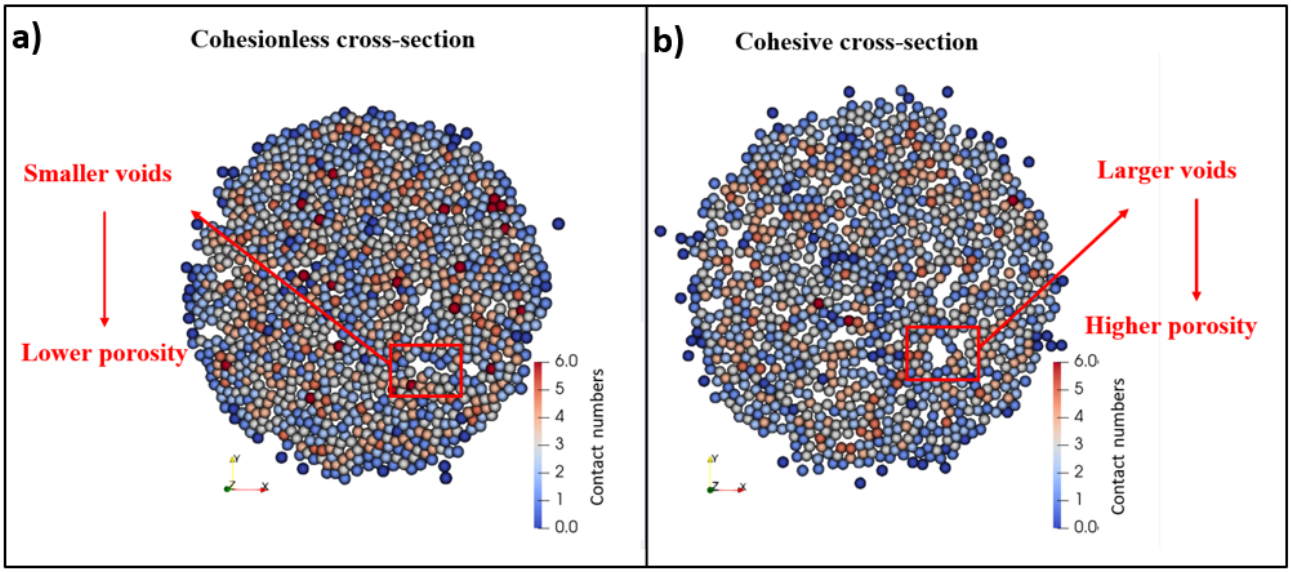

Fig. 7. Extracted cohesionless and cohesive cross-section in DEM (a) μ_r= 0.2, CED = 0 J/m^3 (b) μ_r= 0.2, CED = 5x10^6 J/m^3

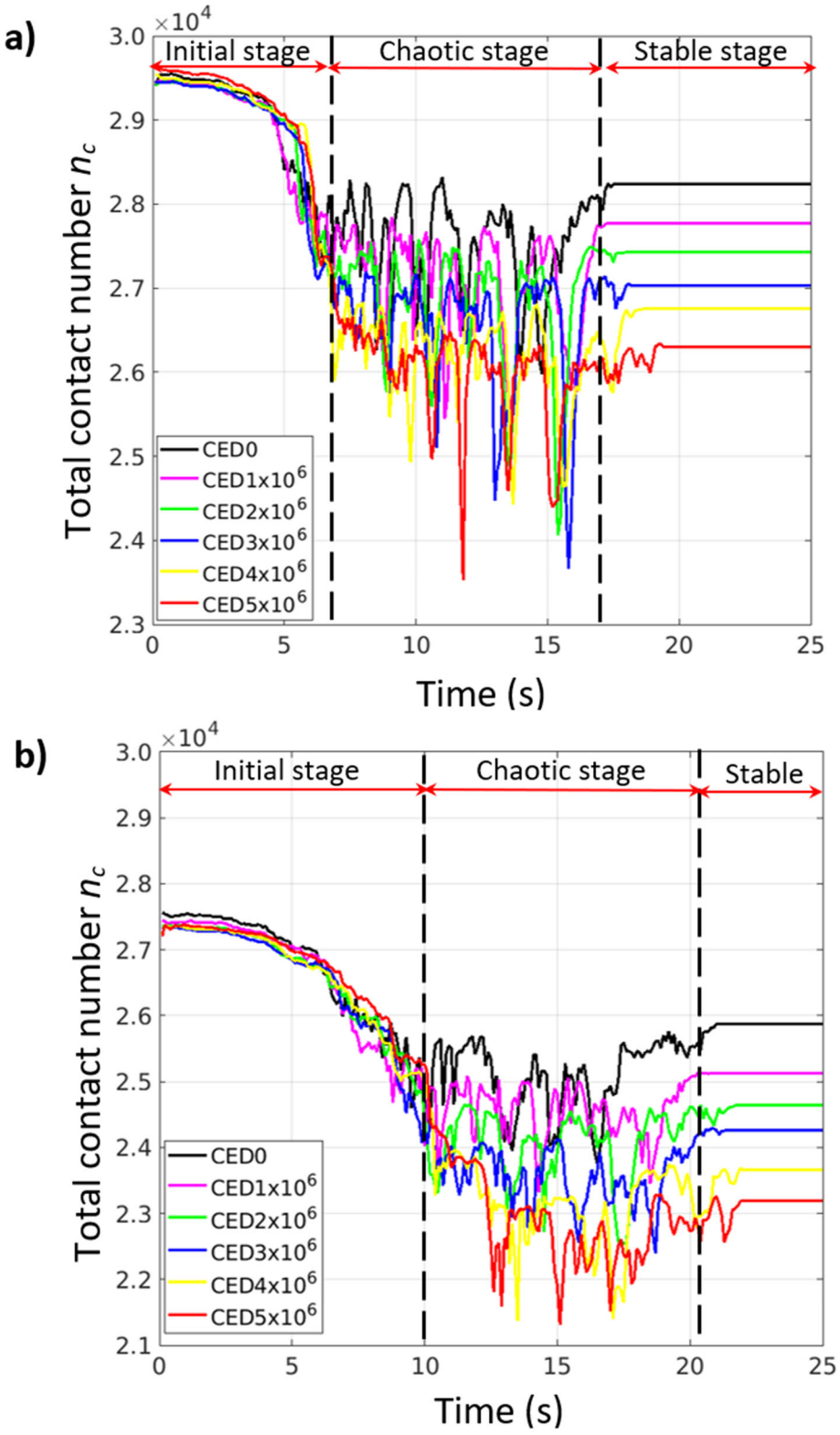

Fig. 8. Contact numbers with different cohesion levels: a) μ_r= 0.1; and b) μ_r = 0.4

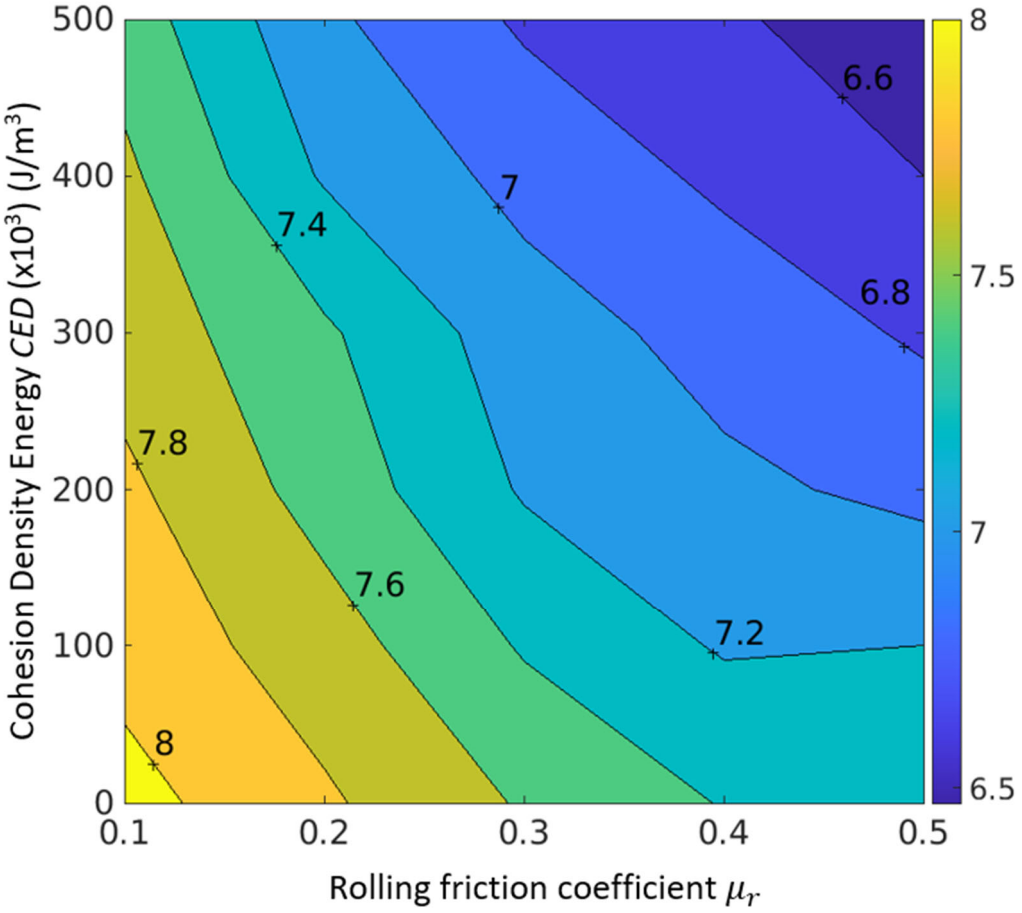

Fig. 9. Mean coordination number as a function of cohesion and rolling friction

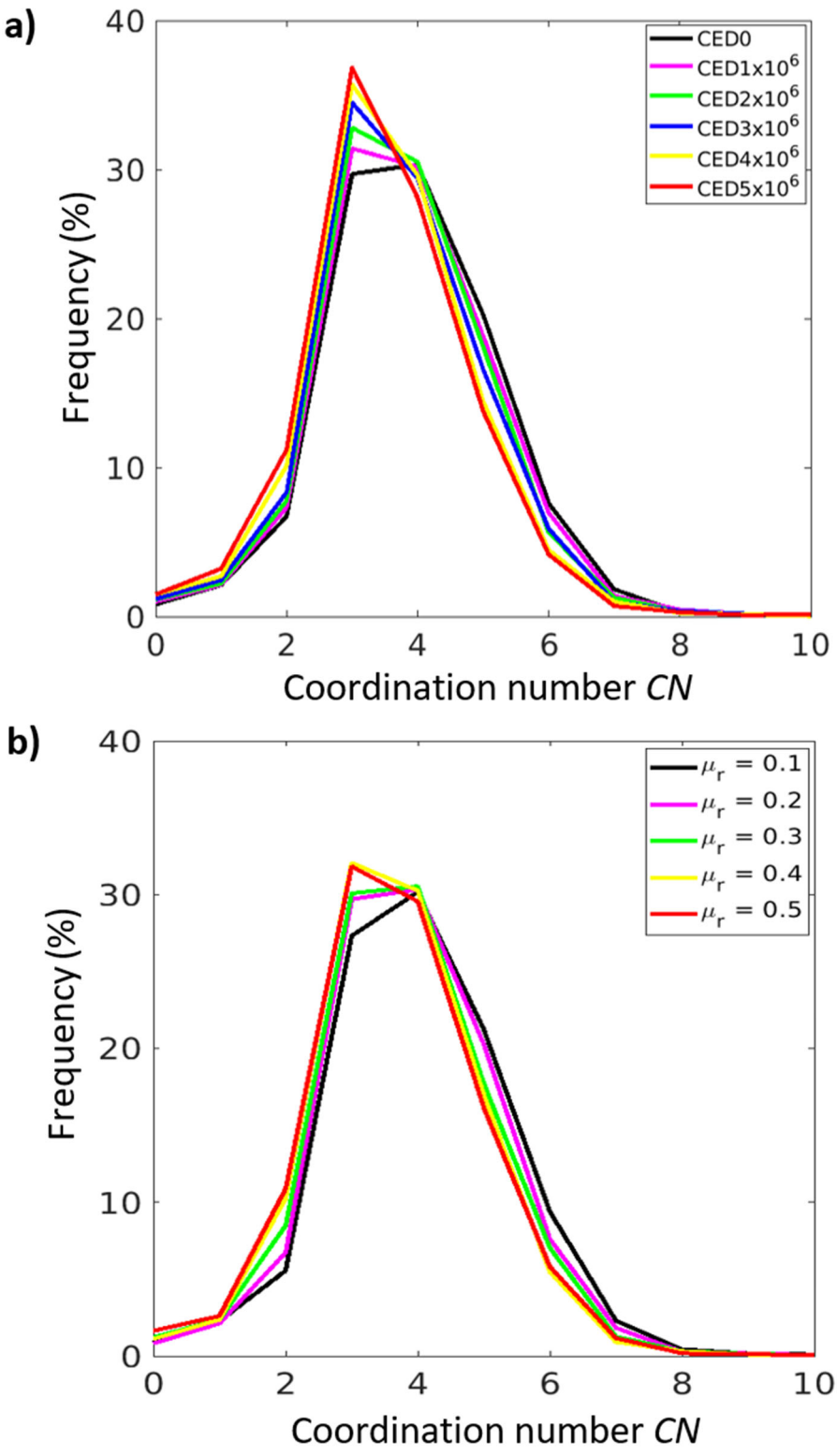

Fig. 10. Frequency of coordination number with (a) varying cohesion levels for μ_r= 0.2; and (b) varying rolling friction for cohesionless case

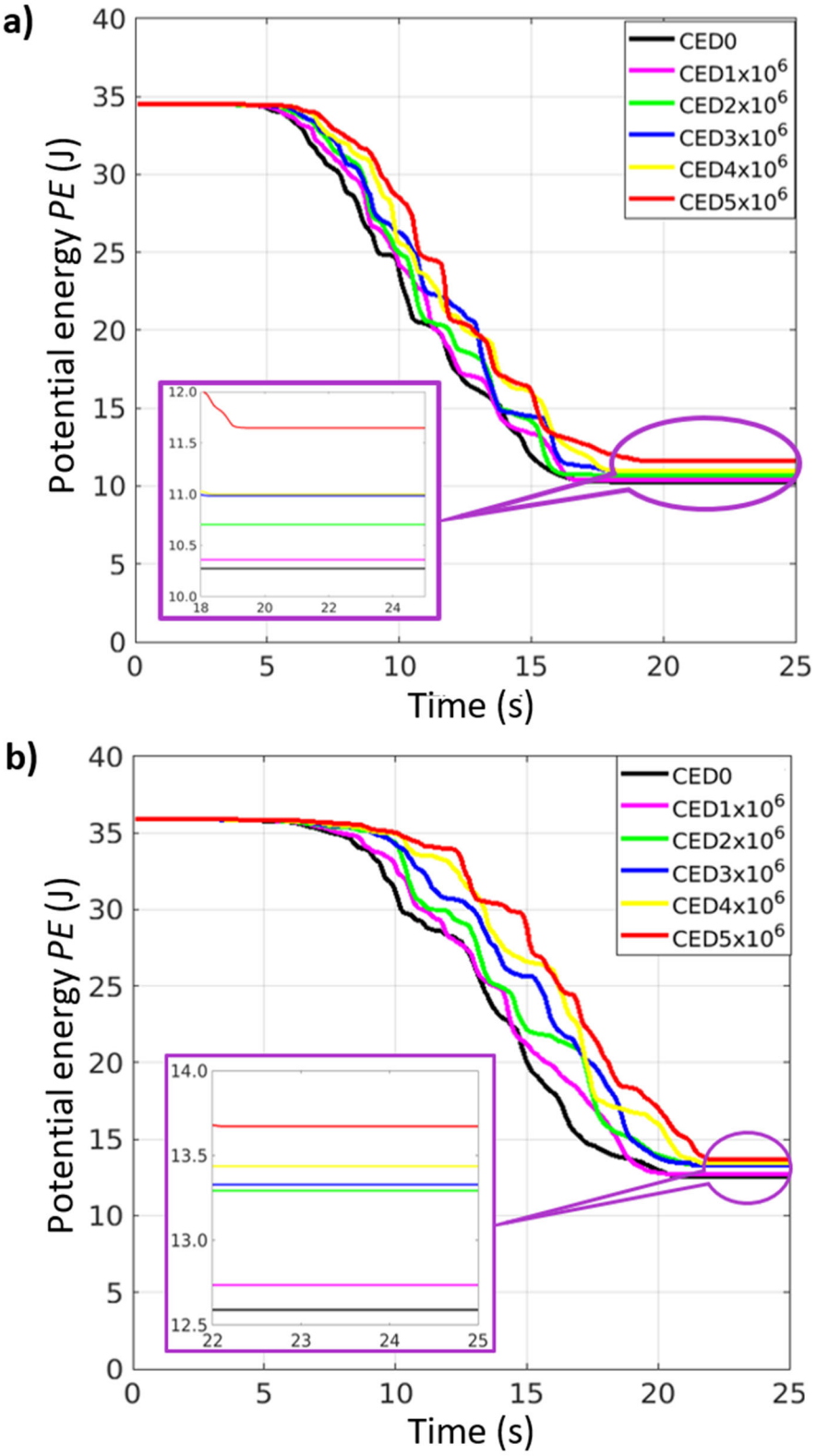

Fig. 11. Potential energy difference with time with varying cohesion levels: for (a) μ_r= 0.1 and (b) μ_r= 0.4

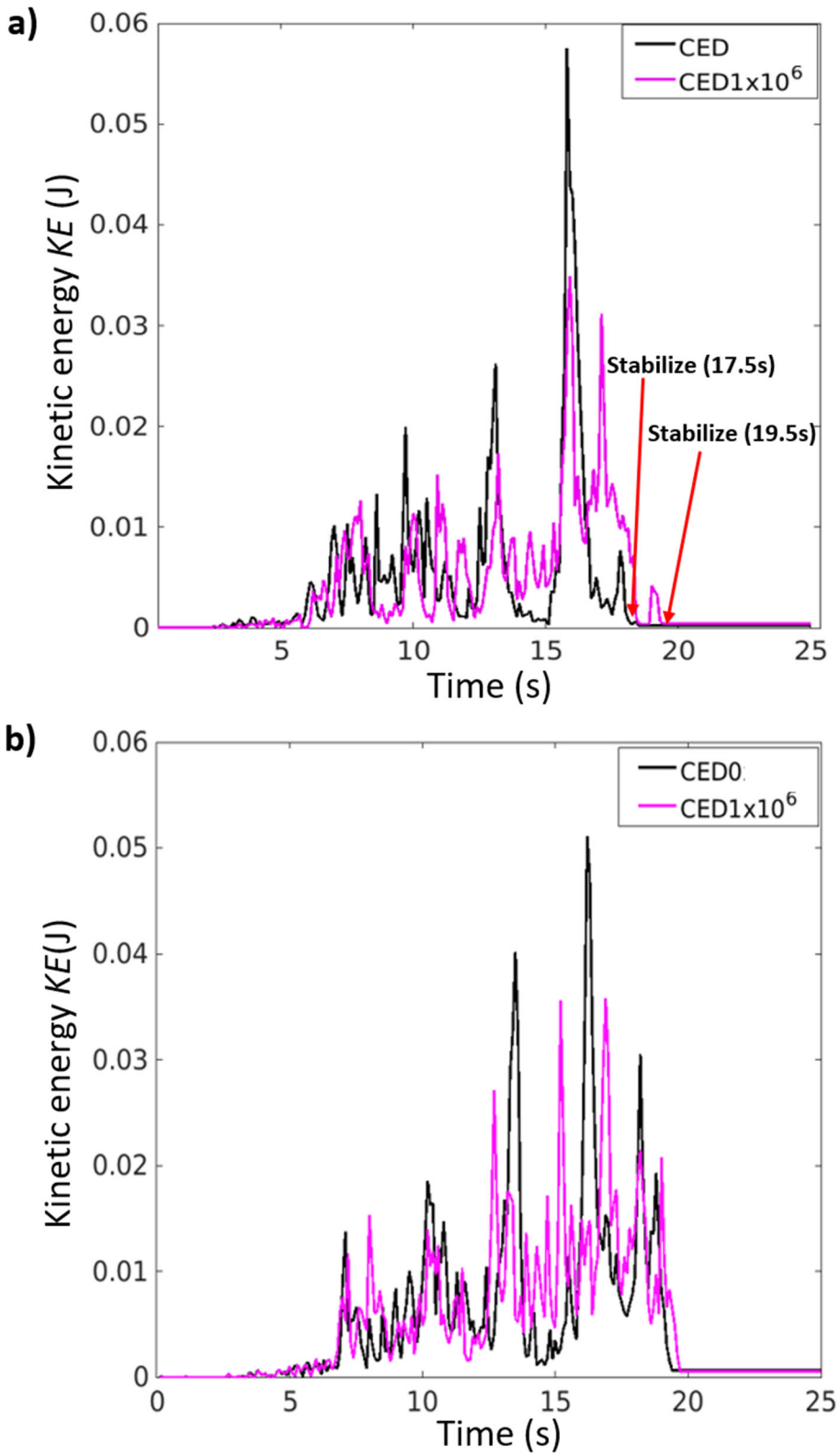

Fig. 12. Variations of average KE with varying cohesion levels: for (a) μ_r= 0.2 and (b) μ_r= 0.3

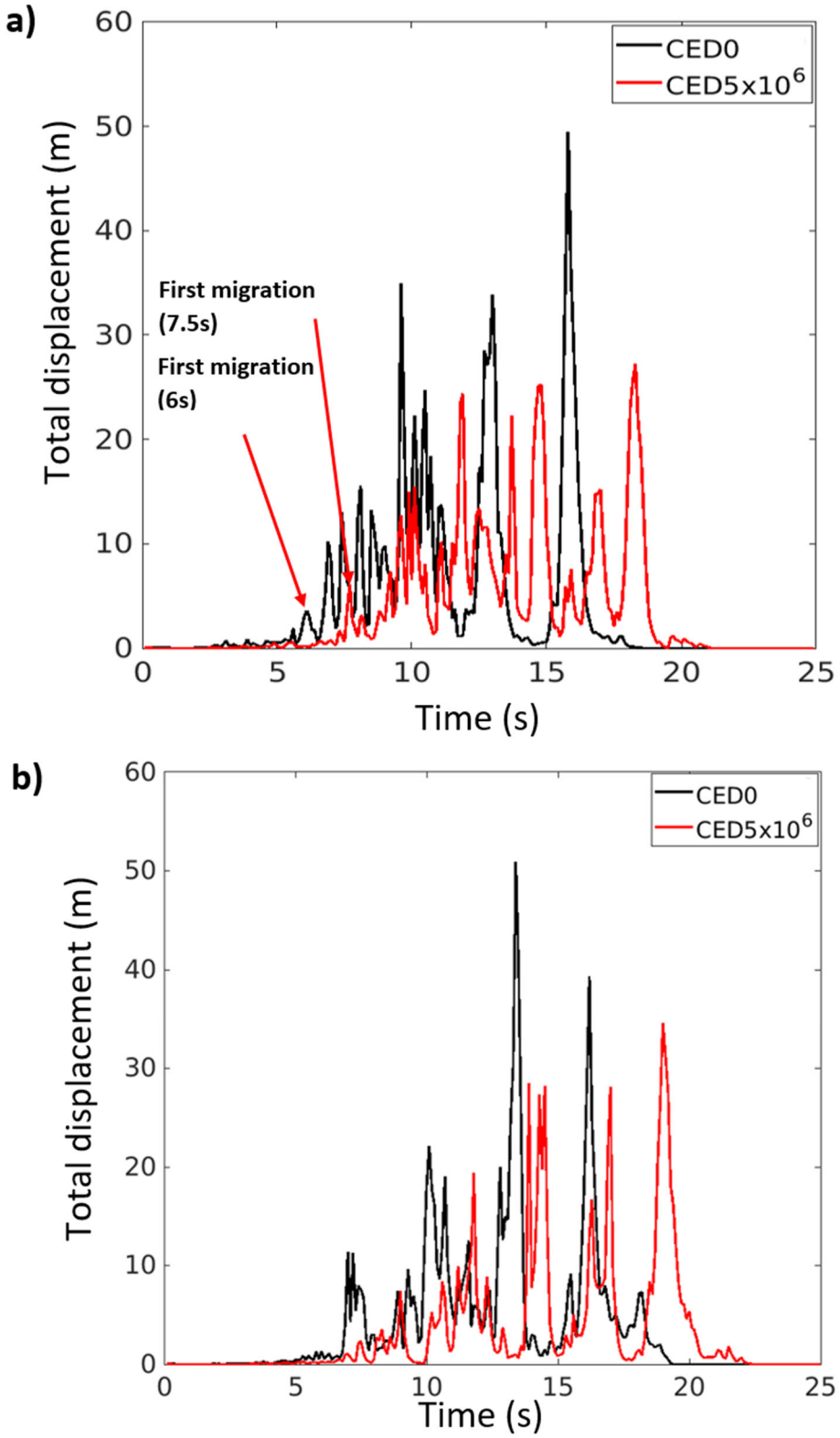

Fig. 13. Variation of the total displacements of particles considering different cohesion levels: for (a) μ_r= 0.2 and (b) μ_r= 0.3

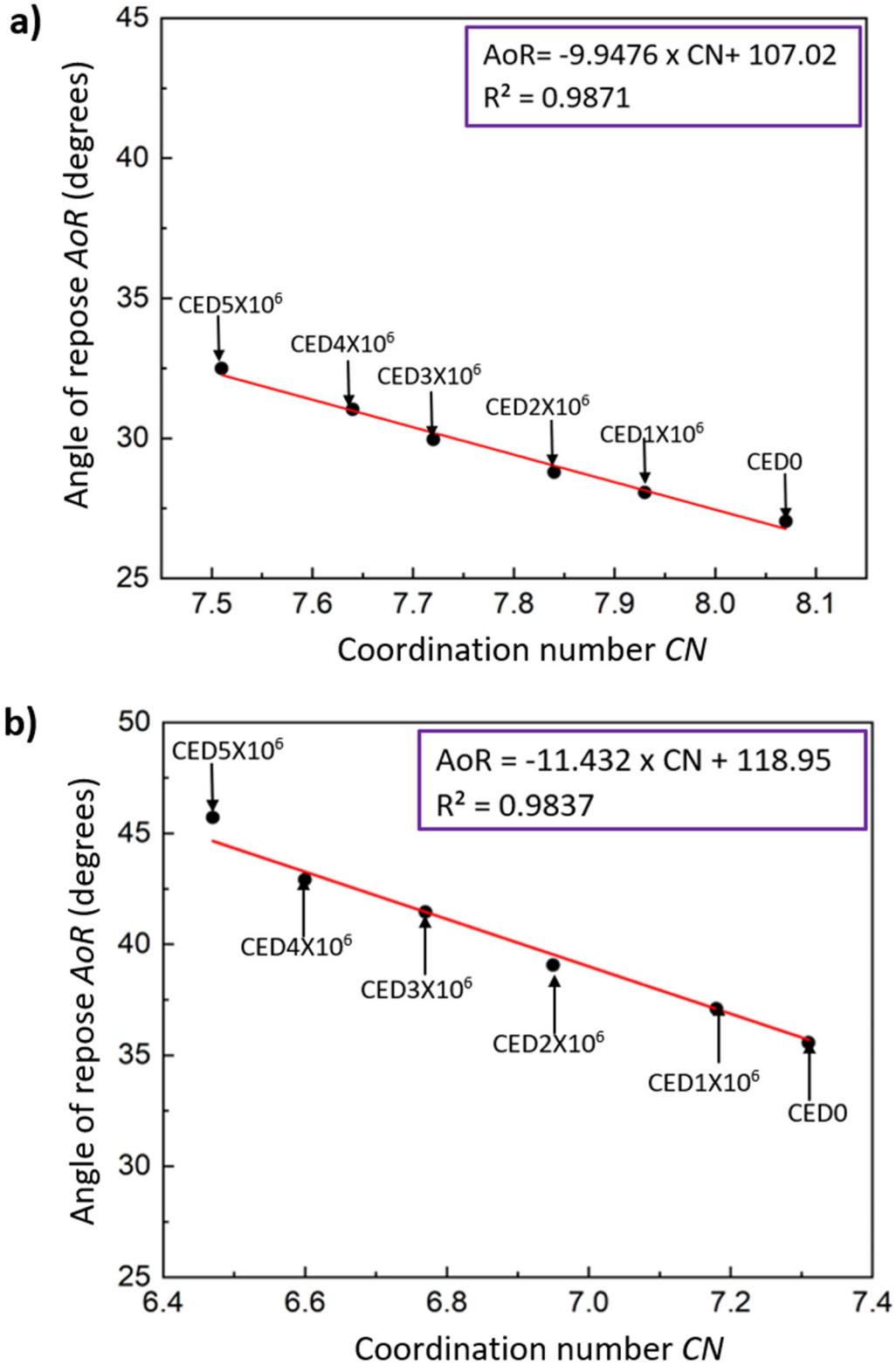

Fig. 14. Correlation between AoR and CN with different cohesion levels: for (a) μ_r= 0.1 and (b) μ_r= 0.5

References

Ai, J., Chen, J.-F., Rotter, J., and Ooi, J. (2011). "Assessment of rolling resistance models in discrete element simulations." *Powder Technol.*, 206, 269-282. https://doi.org/10.1016/j.powtec.2010.09.030.

Amberger, S., Friedl, M., Goniva, C., Pirker, S., and Kloss, C. (2012). "Approximation of Objects by Spheres for Multisphere Simulations in DEM."

Barthel, E. (2008). "Adhesive elastic contacts: JKR and more." *J. Phys*, 41(16), 163001.

Beakawi Al-Hashemi, H. M., and Baghabra Al-Amoudi, O. S. (2018). "A review on the angle of repose of granular materials." *Powder Technol.*, 330, 397-417. https://doi.org/10.1016/j.powtec.2018.02.003.

Behjani, M. A., Rahmanian, N., Fardina bt Abdul Ghani, N., and Hassanpour, A. (2017). "An investigation on process of seeded granulation in a continuous drum granulator using DEM." *Adv Powder Technol*, 28(10), 2456-2464. https://doi.org/10.1016/j.apt.2017.02.011.

Belheine, N., Plassiard, J. P., Donzé, F. V., Darve, F., and Seridi, A. (2009). "Numerical simulation of drained triaxial test using 3D discrete element modeling." *Computers and Geotechnics*, 36(1), 320-331. https://doi.org/10.1016/j.compgeo.2008.02.003.

Campillo, M., Pérez, P., Daher, J., and Pérez, L. (2021). "Percentage porosity computation of three-dimensional non-convex porous geometries using the direct Monte Carlo simulation." *Eng Comput* . 37 https://doi.org/10.1007/s00366-019-00866-2.

Carstensen, J. T., and Chan, P.-C. (1976). "Relation between particle size and repose angles of powders." *Powder Technol.*, 15(1), 129-131. https://doi.org/10.1016/0032-5910(76)80037-X.

Chen, J., and Anandarajah, A. (1996). "Van der Waals Attraction between Spherical Particles." *Journal of Colloid and Interface Science*, 180(2), 519-523. https://doi.org/10.1006/jcis.1996.0332.

Chen, J., Vinod, J. S., Indraratna, B., Ngo, N. T., Gao, R., and Liu, Y. (2022). "A discrete element study on the deformation and degradation of coal-fouled ballast." *Acta Geotech.* 10.1007/s11440-022-01453-4.

Deng, X. L., and Davé, R. N. (2013). "Dynamic simulation of particle packing influenced by size, aspect ratio and surface energy." *Granul. Matter*, 15(4), 401-415. https://doi.org/10.1007/s10035-013-0413-0.

Derakhshani, S. M., Schott, D. L., and Lodewijks, G. (2015). "Micro–macro properties of quartz sand: Experimental investigation and DEM simulation." *Powder Technol.*, 269, 127-138. https://doi.org/10.1016/j.powtec.2014.08.072.

Derjaguin, B. V., Muller, V. M., and Toporov, Y. P. (1975). "Effect of contact deformations on the adhesion of particles." *Journal of Colloid and Interface Science*, 53(2), 314-326. https://doi.org/10.1016/0021-9797(75)90018-1.

Einav, I. (2007). "Fracture propagation in brittle granular matter." *Proc. R. Soc. A: Math. Phys. Eng. Sci.*, 463, 3021-3035. https://doi.org/10.1098/rspa.2007.1898.

El-Kassem, B., Salloum, N., Brinz, T., Heider, Y., and Markert, B. (2021). "A multivariate regression parametric study on DEM input parameters of free-flowing and cohesive powders with experimental data-based validation." *Comput. Part. Mech.*, 8(1), 87-111. https://doi.org/10.1007/s40571-020-00315-8.

El Shamy, U., and Zeghal, M. (2005). "Coupled Continuum-Discrete Model for Saturated Granular Soils." *Journal of Engineering Mechanics*, 131(4), 413-426. 10.1061/(ASCE)0733-9399(2005)131:4(413).

Gentilini, C., Govoni, L., Miranda, S., Gottardi, G., and Ubertini, F. (2012). "Three-dimensional numerical modelling of falling rock protection barriers." *Computers and Geotechnics*, 44, 58–72. https://doi.org/10.1016/j.compgeo.2012.03.011.

Goniva, C., Kloss, C., Deen, N. G., Kuipers, J. A. M., and Pirker, S. (2012). "Influence of rolling friction on single spout fluidized bed simulation." *Particuology*, 10(5), 582-591. https://doi.org/10.1016/j.partic.2012.05.002.

Goudarzy, M., Sarkar, D., Lieske, W., and Wichtmann, T. (2021). "Influence of plastic fines content on the liquefaction susceptibility of sands: monotonic loading." *Acta Geotech.* https://doi.org/10.1007/s11440-021-01283-w.
Gratchev, I. B., Sassa, K., Osipov, V. I., and Sokolov, V. N. (2006). "The liquefaction of clayey soils under cyclic loading." *Eng. Geol.*, 86(1), 70-84. https://doi.org/10.1016/j.enggeo.2006.04.006.
Grima, A. P. (2011). "Quantifying and modelling mechanisms of flow in cohesionless and cohesive granular materials."
Hamaker, H. C. (1937). "The London—van der Waals attraction between spherical particles." *Physica*, 4(10), 1058-1072. https://doi.org/10.1016/S0031-8914(37)80203-7.
Hassanzadeh, V., Wensrich, C. M., and Moreno-Atanasio, R. (2020). "Elucidation of the role of cohesion in the macroscopic behaviour of coarse particulate systems using DEM." *Powder Technol.*, 361, 374-388. https://doi.org/10.1016/j.powtec.2019.07.070.
He, Y., Hassanpour, A., Alizadeh Behjani, M., and Bayly, A. E. (2021). "A novel stiffness scaling methodology for discrete element modelling of cohesive fine powders." *Appl. Math. Model.*, 90, 817-844. https://doi.org/10.1016/j.apm.2020.08.062.
Hertz, H. (1881). "On the contact of elastic solids." *Z. Reine Angew. Mathematik*, 92, 156-171.
Hoshishima, C., Ohsaki, S., Nakamura, H., and Watano, S. (2021). "Parameter calibration of discrete element method modelling for cohesive and non-spherical particles of powder." *Powder Technol.*, 386, 199-208. https://doi.org/10.1016/j.powtec.2021.03.044.
Huang, H., and Tutumluer, E. (2011). "Discrete Element Modeling for fouled railroad ballast." *Construction and Building Materials*, 25(8), 3306-3312. https://doi.org/10.1016/j.conbuildmat.2011.03.019.
Indraratna, B., Phan Nghi, M., Nguyen Thanh, T., and Huang, J. (2021). "Simulating Subgrade Soil Fluidization Using LBM-DEM Coupling." *Int. J. Geomech.*, 21(5), 04021039. 10.1061/(ASCE)GM.1943-5622.0001997.
Iwashita, K., and Oda, M. (1998). "Rolling Resistance at Contacts in Simulation of Shear Band Development by DEM." *Journal of Engineering Mechanics*, 124(3), 285-292. 10.1061/(ASCE)0733-9399(1998)124:3(285).
Johnson, K. L., and Greenwood, J. A. (1997). "An Adhesion Map for the Contact of Elastic Spheres." *Journal of Colloid and Interface Science*, 192(2), 326-333. https://doi.org/10.1006/jcis.1997.4984.
Johnson, K. L., Kendall, K., Roberts, A. D., and Tabor, D. (1971). "Surface energy and the contact of elastic solids." *Proc. R. Soc. A: Math. Phys. Sci.*, 324(1558), 301-313. https://doi.org/10.1098/rspa.1971.0141.
Kermani, E., Qiu, T., and Li, T. (2015). "Simulation of Collapse of Granular Columns Using the Discrete Element Method." *Int. J. Geomech.*, 15(6), 04015004. 10.1061/(ASCE)GM.1943-5622.0000467.
Kloss, C., and Goniva, C. (2011). "LIGGGHTS – Open Source Discrete Element Simulations of Granular Materials Based on Lammps." *Supplemental Proceedings*, 781-788.
Lajeunesse, E., Mangeney-Castelnau, A., and Vilotte, J. P. (2004). "Spreading of a granular mass on a horizontal plane." *Phys. Fluids*, 16(7), 2371-2381. https://doi.org/10.1063/1.1736611.
Li, S., Marshall, J. S., Liu, G., and Yao, Q. (2011). "Adhesive particulate flow: The discrete-element method and its application in energy and environmental engineering." *Prog. Energy Combust. Sci.*, 37(6), 633-668. https://doi.org/10.1016/j.pecs.2011.02.001.
Li, Y., Xu, Y., and Thornton, C. (2005). "A comparison of discrete element simulations and experiments for 'sandpiles' composed of spherical particles." *Powder Technol.*, 160(3), 219-228. https://doi.org/10.1016/j.powtec.2005.09.002.
Liu, Y., Liu, H., and Mao, H. (2018). "The influence of rolling resistance on the stress-dilatancy and fabric anisotropy of granular materials." *Granul. Matter*, 20 https://doi.org/.1007/s10035-017-0780-z.
Lommen, S., Schott, D., and Lodewijks, G. (2014). "DEM speedup: Stiffness effects on behavior of bulk material." *Particuology*, 12, 107-112. https://doi.org/10.1016/j.partic.2013.03.006.
Louati, H., Bednarek, X., Martin, S., Ndiaye, A., and Bonnefoy, O. (2019). "Qualitative and quantitative DEM analysis of cohesive granular material behaviour in FT4 shear tester." *Chem Eng Res Des.*, 148, 155-163. https://doi.org/10.1016/j.cherd.2019.05.059.

Mason, T., Levine, A., Ertaş, D., and Halsey, T. T. C. (1999). "Critical angle of wet sandpiles." *Phys Rev E Stat Phys Plasmas Fluids Relat Interdiscip Topics.*, 60, R5044-5047. https://doi.org/10.1103/PhysRevE.60.R5044.

Matsusaka, S., Maruyama, H., Matsuyama, T., and Ghadiri, M. (2010). "Triboelectric charging of powders: A review." *Chem. Eng. Sci.*, 65(22), 5781-5807. https://doi.org/10.1016/j.ces.2010.07.005.

Meier, C., Weissbach, R., Weinberg, J., Wall, W. A., and John Hart, A. (2019). "Modeling and characterization of cohesion in fine metal powders with a focus on additive manufacturing process simulations." *Powder Technol.*, 343, 855-866. https://doi.org/10.1016/j.powtec.2018.11.072.

Mitarai, N., and Nori, F. (2006). "Wet granular materials." *Adv. Phys.*, 55(1-2), 1-45. https://doi.org/10.1080/00018730600626065.

Muftah, A., and Gutierrez, M. (2010). "Comprehensive study of the effects of rolling resistance on the stress–strain and strain localization behavior of granular materials." *Granul. Matter*, 12, 527-541. https://doi.org/10.1007/s10035-010-0211-x.

Nakashima, H., Shioji, Y., Kobayashi, T., Aoki, S., Shimizu, H., Miyasaka, J., and Ohdoi, K. (2011). "Determining the angle of repose of sand under low-gravity conditions using discrete element method." *J. Terramechanics.*, 48(1), 17-26. https://doi.org/10.1016/j.jterra.2010.09.002.

Nase, S. T., Vargas, W. L., Abatan, A. A., and McCarthy, J. J. (2001). "Discrete characterization tools for cohesive granular material." *Powder Technol.*, 116(2), 214-223. https://doi.org/10.1016/S0032-5910(00)00398-3.

Nguyen, N. H. T., Bui, H. H., and Nguyen, G. D. (2020). "Effects of material properties on the mobility of granular flow." *Granul. Matter*, 22(3), 59. https://doi.org/10.1007/s10035-020-01024-y.

Nguyen, N. H. T., Bui, H. H., Nguyen, G. D., and Kodikara, J. (2017). "A cohesive damage-plasticity model for DEM and its application for numerical investigation of soft rock fracture properties." *Int. J. Plast.*, 98, 175-196. https://doi.org/10.1016/j.ijplas.2017.07.008.

Nguyen, T. T., and Indraratna, B. (2020). "A Coupled CFD–DEM Approach to Examine the Hydraulic Critical State of Soil under Increasing Hydraulic Gradient." *Int. J. Geomech.*, 20(9), 04020138. https://doi.org/10.1061/(ASCE)GM.1943-5622.0001782.

Nguyen, T. T., and Indraratna, B. (2020). "The energy transformation of internal erosion based on fluid-particle coupling." *Computers and Geotechnics*, 121, 103475. https://doi.org/10.1016/j.compgeo.2020.103475.

Nguyen, T. T., and Indraratna, B. (2020). "The role of particle shape on hydraulic conductivity of granular soils captured through Kozeny–Carman approach." *Géotechnique Letters*, 10(3), 398-403. https://doi.org/10.1680/jgele.20.00032.

O'Sullivan, C. (2011). "Particle-Based Discrete Element Modeling: Geomechanics Perspective." *Int. J. Geomech.*, 11(6), 449-464. https://doi.org/10.1061/(ASCE)GM.1943-5622.0000024.

Parteli, E. J. R., Schmidt, J., Blümel, C., Wirth, K.-E., Peukert, W., and Pöschel, T. (2014). "Attractive particle interaction forces and packing density of fine glass powders." *Sci. Rep.*, 4(1), 6227. https://doi.org/10.1038/srep06227.

Phan, Q. T., Bui, H. H., Nguyen, G. D., and Bouazza, A. (2021). "Effect of particle rolling resistance on drained and undrained behaviour of silty sand." *Acta Geotech.*, 16(8), 2657-2682. https://doi.org/10.1007/s11440-020-01128-y.

Potyondy, D. O., and Cundall, P. A. (2004). "A bonded-particle model for rock." *Int. J. Rock Mech. Min.*, 41(8), 1329-1364. https://doi.org/10.1016/j.ijrmms.2004.09.011.

Prokopovich, P., and Perni, S. (2011). "Comparison of JKR- and DMT-based multi-asperity adhesion model: Theory and experiment." *Colloids Surf, A Physicochem Eng Asp*, 383(1), 95-101. https://doi.org/10.1016/j.colsurfa.2011.01.011.

Rackl, M., Grötsch, F. E., Rusch, M., and Fottner, J. (2017). "Qualitative and quantitative assessment of 3D-scanned bulk solid heap data." *Powder Technol.*, 321, 105-118. https://doi.org/10.1016/j.powtec.2017.08.009.

Roessler, T., and Katterfeld, A. (2019). "DEM parameter calibration of cohesive bulk materials using a simple angle of repose test." *Particuology*, 45, 105-115. https://doi.org/10.1016/j.partic.2018.08.005.

Rognon, P., Roux, J.-N., Wolf, D., Naaim, M., and Chevoir, F. (2007). "Rheophysics of cohesive granular materials." *EPL (Europhysics Letters)*, 74, 644. https://doi.org/10.1209/epl/i2005-10578-y.
Roy, S., Singh, A., Luding, S., and Weinhart, T. (2016). "Micro–macro transition and simplified contact models for wet granular materials." *Comput. Part. Mech.*, 3(4), 449-462. https://doi.org/10.1007/s40571-015-0061-8.
Rumpf, H. "The strength of granules and agglomerates." *Proc., Agglomeration-Proceedings of the First International Symposium on Agglomeration, Philadelphia, 1962*, 379-418.
Schwarze, R., Gladkyy, A., Uhlig, F., and Luding, S. (2013). "Rheology of weakly wetted granular materials: a comparison of experimental and numerical data." *Granul. Matter*, 15(4), 455-465. https://doi.org/10.1007/s10035-013-0430-z.
Shan, T., and Zhao, J. (2014). "A coupled CFD-DEM analysis of granular flow impacting on a water reservoir." *Acta Mech.*, 225(8), 2449-2470. https://doi.org/10.1007/s00707-014-1119-z.
Tao, J., and Tao, H. (2017). "Factors Affecting Piping Erosion Resistance: Revisited with a Numerical Modeling Approach." *Int. J. Geomech.*, 17 10.1061/(ASCE)GM.1943-5622.0000999.
Terzaghi, K. (1943). *Theoretical Soil Mechanics*, Wiley, New York.
Thakur, S. C., Morrissey, J. P., Sun, J., Chen, J. F., and Ooi, J. Y. (2014). "Micromechanical analysis of cohesive granular materials using the discrete element method with an adhesive elasto-plastic contact model." *Granul. Matter*, 16(3), 383-400. https://doi.org/10.1007/s10035-014-0506-4.
Thoeni, K., Giacomini, A., Lambert, C., Sloan, S. W., and Carter, J. P. (2014). "A 3D discrete element modelling approach for rockfall analysis with drapery systems." *Int. J. Rock Mech. Min.*, 68, 107-119. https://doi.org/10.1016/j.ijrmms.2014.02.008.
Thornton, C. (2000). "Numerical simulations of deviatoric shear deformation of granular media." *Géotechnique*, 50(1), 43-53. 10.1680/geot.2000.50.1.43.
Ucgul, M., Fielke, J. M., and Saunders, C. (2014). "Three-dimensional discrete element modelling of tillage: Determination of a suitable contact model and parameters for a cohesionless soil." *Biosyst. Eng.*, 121, 105-117. https://doi.org/10.1016/j.biosystemseng.2014.02.005.
Wensrich, C. M., and Katterfeld, A. (2012). "Rolling friction as a technique for modelling particle shape in DEM." *Powder Technol.*, 217, 409-417. https://doi.org/10.1016/j.powtec.2011.10.057.
Wiącek, J., Molenda, M., Ooi, J. Y., and Favier, J. (2012). "Experimental and numerical determination of representative elementary volume for granular plant materials." *Granul. Matter*, 14(4), 449-456. https://doi.org/10.1007/s10035-012-0351-2.
Wu, S., Chen, Y., Zhu, Y., Zhang, P., Scheuermann, A., Jin, G., and Zhu, W. (2021). "Study on filtration process of geotextile with LBM-DEM-DLVO coupling method." *Geotextiles and Geomembranes*, 49(1), 166-179. https://doi.org/10.1016/j.geotexmem.2020.09.011.
Xu, J. Q., Zou, R. P., and Yu, A. B. (2007). "Analysis of the packing structure of wet spheres by Voronoi–Delaunay tessellation." *Granul. Matter*, 9(6), 455-463. https://doi.org/10.1007/s10035-007-0052-4.
Yang, R. Y., Zou, R. P., and Yu, A. B. (2000). "Computer simulation of the packing of fine particles." *Phys. Rev.*, 62(3), 3900-3908. https://doi.org/10.1103/PhysRevE.62.3900.
Yimsiri, S., and Soga, K. (2010). "DEM analysis of soil fabric effects on behaviour of sand." *Géotechnique*, 60(6), 483-495. https://doi.org/10.1680/geot.2010.60.6.483.
Yin, Y., Cui, Y., Tang, Y., Liu, D., Lei, M., and Chan, D. (2021). "Solid–fluid sequentially coupled simulation of internal erosion of soils due to seepage." *Granul. Matter*, 23 10.1007/s10035-020-01076-0.
Yu, A., Liu, L., Zhang, Z., Yang, R., and Zou, R. (2003). "Computer simulation of the packing of particles." *International Journal of Materials & Product Technology - INT J MATER PROD TECHNOL*, 19 https://doi.org/10.1504/IJMPT.2003.002516.
Yu, A. B., Feng, C. L., Zou, R. P., and Yang, R. Y. (2003). "On the relationship between porosity and interparticle forces." *Powder Technol.*, 130(1), 70-76. https://doi.org/10.1016/S0032-5910(02)00228-0.
Zhao, J., and Shan, T. (2013). "Coupled CFD–DEM simulation of fluid–particle interaction in geomechanics." *Powder Technol.*, 239, 248-258. https://doi.org/10.1016/j.powtec.2013.02.003.

Zhou, B., Wang, J., and Wang, H. (2017). "Three-dimensional sphericity, roundness and fractal dimension of sand particles." *Géotechnique*, 68(1), 18-30. https://doi.org/10.1680/jgeot.16.P.207.

Zhou, Y. C., Wright, B. D., Yang, R. Y., Xu, B. H., and Yu, A. B. (1999). "Rolling friction in the dynamic simulation of sandpile formation." *Phys. A: Stat. Mech. Appl.*, 269(2), 536-553. https://doi.org/10.1016/S0378-4371(99)00183-1.

Zhou, Y. C., Xu, B., Yu, A., and Zulli, P. (2001). "Numerical investigation of the angle of repose of monosized spheres." *Phys. Rev. E Stat. Nonlin. Soft Matter Phys.*, 64, 021301. https://doi.org/10.1103/PhysRevE.64.021301.

Zhu, H. P., Zhou, Z. Y., Yang, R. Y., and Yu, A. B. (2007). "Discrete particle simulation of particulate systems: Theoretical developments." *Chem. Eng. Sci.*, 62(13), 3378-3396. https://doi.org/10.1016/j.ces.2006.12.089.